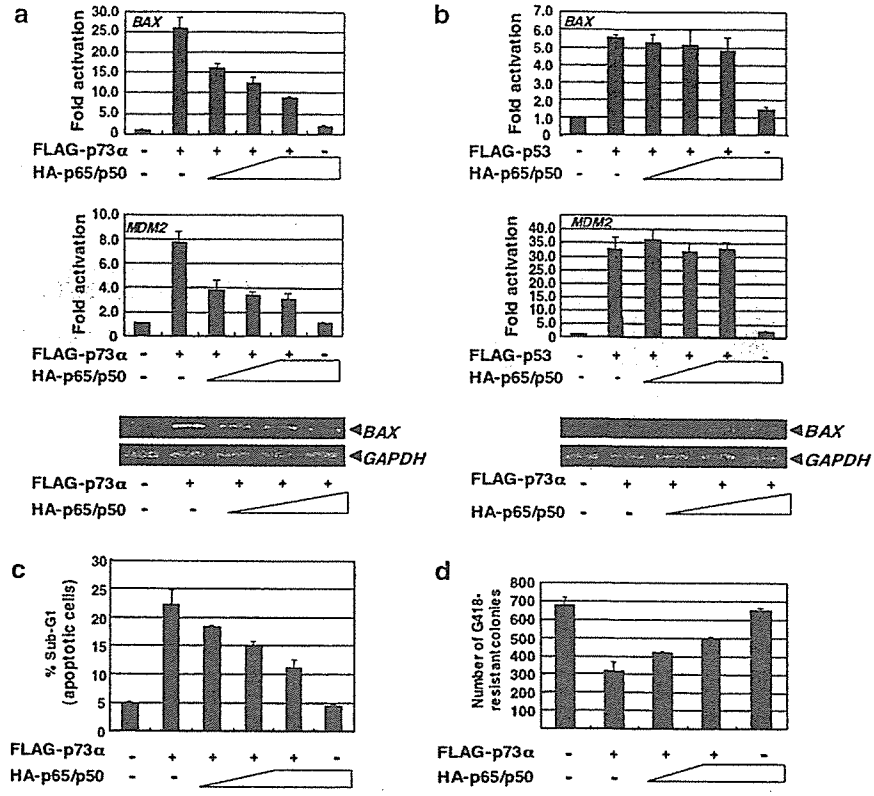

Figure 6 NF-κB inhibits the transcriptional as well as proapoptotic activity of p73. (**a** and **b**) NF-κB-mediated inhibition of the p73α-dependent transactivation but not of p53. H1299 cells were co-transfected with 25 ng of the expression plasmid for FLAG-p73α (**a**) or FLAG-p53 (**b**) together with 100 ng of the luciferase reporter construct, which carries the p53/p73-responsive element derived from *BAX* or *MDM2* promoter and 10 ng of the *Renilla* luciferase plasmid (pRL-TK) in the presence or absence of the increasing amounts of HA-p65 and HA-p50 expression plasmids (50, 100, or 200 ng). All transfections were performed in triplicate. At 48 h after transfection, cells were analysed for their luciferase activities. Firefly luminescence signal was normalized based on the *Renilla* luminescence signal. Results were shown as fold induction of the firefly luciferase activity compared with control cells transfected with the empty plasmid alone. For RT–PCR analysis, H1299 cells were co-transfected with the FLAG-p73α or FLAG-p53 expression plasmid together with or without the increasing amounts of the HA-p65 and HA-p50 expression plasmids. At 48 h post-transfection, total RNA was subjected to RT–PCR analysis for the expression of *BAX*. Amplification of *GAPDH* serves as an internal control. (**c**) FACS analysis. H1299 cells were co-transfected with the constant amount of the expression plasmid encoding FLAG-p73α together with or without the increasing amounts of the HA-p65 and HA-p50 expression plasmids. At 48 h after transfection, cells were fixed and stained with propidium iodide. (**d**) Colony formation assay. H1299 cells were co-transfected with the indicated combinations of the expression plasmids. At 24 h after transfection, cells were selected with G418 (400 μg/ml) for 2 weeks. The number of G418-resistant colonies was scored.

colony formation assays demonstrated that co-expression of FLAG-p73α with the increasing amounts of the HA-p65 and HA-p50 increases number of G418-resistant colonies as compared with that in cells expressing FLAG-p73α alone (Figure 6d). Taken together, these results strongly suggest that NF-κB has an ability to inhibit the transcriptional activity as well as proapoptotic function of p73α.

NF-κB does not bind to p73α in cells

To investigate how NF-κB decreases the stability and activity of p73α, we examined whether NF-κB could bind to p73α. H1299 cells were co-transfected with the indicated combinations of the expression plasmids. At 48 h after transfection, whole-cell lysates were immunoprecipitated with the anti-FLAG or anti-HA antibody followed by immunoblotting with the anti-HA or anti-p73 antibody, respectively. As shown in Figure 7a, the anti-FLAG immunoprecipitates did not contain HA-p65 and HA-p50. Similarly, FLAG-p73α was not co-immunoprecipitated with HA-p65 and HA-p50 (Figure 7b). Under our experimental conditions, FLAG-p73α was co-immunoprecipitated with MDM2 (data not shown), which was consistent with the previous reports (Balint *et al*., 1999; Zeng *et al*., 1999). Thus, it is likely that NF-κB-mediated inhibitory effects on p73α might be indirect without a direct interaction between them.

Transactivation function of NF-κB is required for the downregulation of p73α

To determine the molecular mechanism by which NF-κB contributes to the degradation of p73α, we focused on the COOH-terminal transactivation domain of p65 (Figure 7c). We generated a deletion mutant of p65 (HA-p65ΔC), which retains a nuclear localization signal but lacks a COOH-terminal transactivation domain. To assess the transactivation function of p65ΔC, we

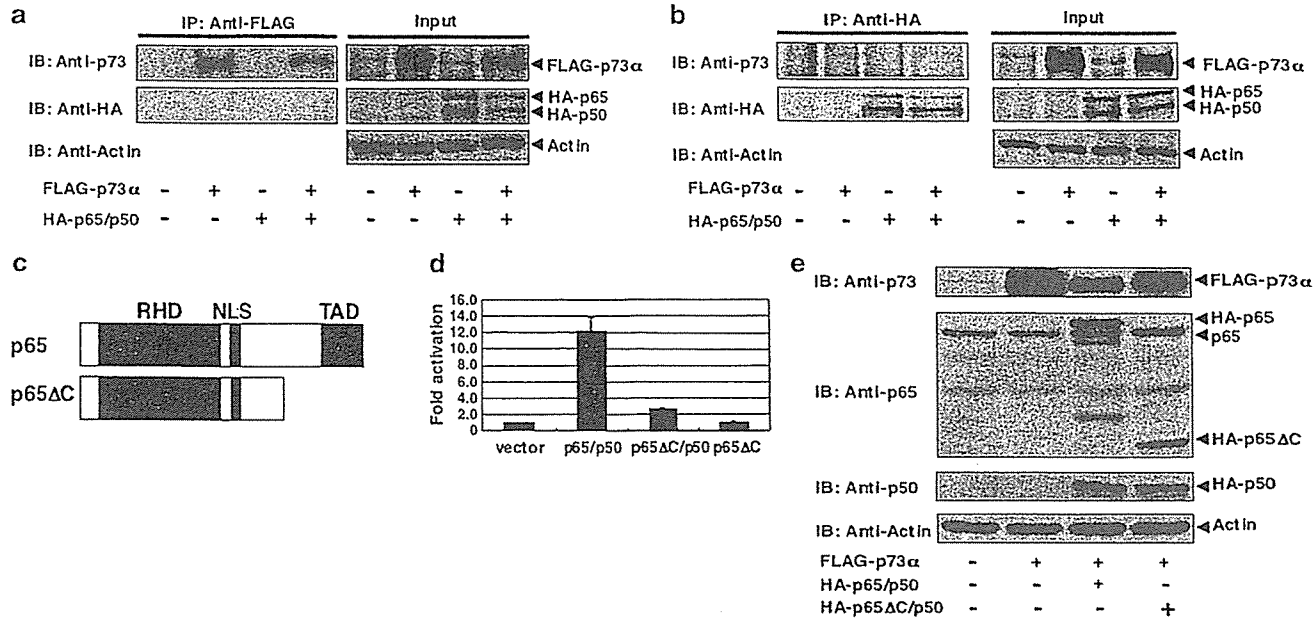

Figure 7 Transcriptional activity of NF-κB is required for the down regulation of p73. (**a** and **b**) Immunoprecipitation experiments. H1299 cells were co-transfected with the indicated combinations of the expression plasmids. At 48 h after transfection, whole-cell lysates were immunoprecipitated with the anti-FLAG (**a**) or with anti-HA (**b**) antibody, followed by immunoblotting with the indicated antibodies. Aliquots of whole-cell lysates were subjected to immunoblotting with the anti-FLAG or with the anti-HA antibody to monitor the expression levels of FLAG-p73α, HA-p65 and HA-p50 (right panels). (**c**) Schematic drawing of the full-length p65 and the COOH-terminal deletion mutant, p65ΔC. RHD, Rel homology domain; NLS, nuclear localization signal; TAD, transactivation domain. (**d**) p65ΔC lacks the transcriptional activity. H1299 cells were co-transfected with the NF-κB-responsive luciferase reporter plasmid and pRL-TK *Renilla* luciferase cDNA together with the empty plasmid, HA-p65 plus HA-p50, HA-p65ΔC plus HA-p50 or HA-p65ΔC. At 48 h after transfection, the luciferase activities were measured. (**e**) Downregulation of p73α is induced by the full-length p65 but not by p65ΔC. H1299 cells were co-transfected with the expression plasmid for FLAG-p73α together with HA-p65 plus HA-p50 or HA-p65ΔC plus HA-p50. At 48 h post-transfection, whole-cell lysates were processed for immunoblotting with the indicated antibodies. Actin was used to confirm that an equivalent amount of protein was loaded into each lane.

performed the luciferase reporter assay. As shown in Figure 7d, HA-p65ΔC alone failed to drive transcription from the NF-κB luciferase reporter, whereas two- to three-fold increase in the luciferase activity was detectable in cells expressing exogenous HA-p65ΔC and HA-p50, which might be due to the complex formation between the endogenous p65 and HA-p50. We then examined the possible effects of HA-p65ΔC on the expression level of FLAG-p73α. H1299 cells were co-transfected with the indicated combinations of the expression plasmids, and whole-cell lysates were analysed for the expression level of FLAG-p73α by immunoblotting. As shown in Figure 7e, WT p65 significantly reduced the amount of FLAG-p73α, whereas HA-p65ΔC had an ability to stabilize FLAG-p73α. Collectively, these results strongly suggest that the transactivation property of NF-κB is required for the degradation of p73α.

Discussion

In the present study, we have found for the first time that NF-κB promotes the ubiquitin-dependent proteasomal turnover of p73 in the absence of a direct physical interaction between them, and also demonstrated that the transcriptional activity of NF-κB is required for this process. In contrast, NF-κB had negligible effects on p53 and p63. Thus, it is likely that the NF-κB-mediated degradation of p73 contributes to the protection of cells from p73-dependent apoptosis. To our knowledge, this is the first report describing the detailed properties of the NF-κB-dependent inhibitory mechanism of p73 function.

Genotoxic stresses increase the stability of p73 and enhance its proapoptotic activity in a pathway dependent on c-Abl (Agami *et al.*, 1999; Gong *et al.*, 1999; Yuan *et al.*, 1999). Intriguingly, Kawai *et al.* (2002) reported that c-Abl phosphorylates IκBα at Tyr-305 to increase its stability, and thereby inhibiting the nuclear translocation and activation of NF-κB, suggesting that the inactivation of NF-κB contributes to the c-Abl-mediated apoptosis. Additionally, it has been demonstrated that, during the cisplatin-mediated apoptosis in hepatocellular carcinoma cells, the downregulation of NF-κB transcriptional activity is correlated with the accumulation of p73 (Kim *et al.*, 2004). In contrast to the DNA-damaging agents that activate c-Abl, TNF-α treatment had undetectable effect on c-Abl (Kharbanda *et al.*, 1995). According to our present results, the activation of the endogenous NF-κB induced by TNF-α resulted in a significant decrease in the stability of p73α. Taken together, it is likely that c-Abl plays an important role in the regulation of NF-κB-mediated destabilization of p73.

Since we could not detect the physical interaction between NF-κB and p73α, NF-κB might regulate p73α stability through an indirect mechanism. Deletion analysis revealed that p65ΔC fails to reduce the amount of p73α, raising a possibility that the transactivation function of NF-κB might be required for the degradation of p73α, and that there could exist an unidentified E3 ubiquitin ligase(s) among the direct targets of NF-κB. Recently, Rossi *et al.* (2005) described that an HECT-type E3 ubiquitin ligase Itch binds to p73, and promotes its degradation through the ubiquitin–proteasome pathway. In contrast, Itch had no detectable effect on p53. Additionally, it has been shown that Jun kinase regulates the TNF-α-mediated apoptosis through the activation of Itch (Chang *et al.*, 2006). Although the examination of the human *Itch* promoter region showed the presence of several putative DNA-binding sites of NF-κB, the enforced expression of NF-κB or TNF-α-mediated activation of the endogenous NF-κB failed to induce the endogenous *Itch* as examined by RT–PCR (data not shown). Considering that p53 is targeted for ubiquitination not only by MDM2 but also by Pirh2 (Leng *et al.*, 2003), it is likely that an as yet unidentified E3 ubiquitin ligase(s) distinct from Itch might be involved in the NF-κB-mediated degradation of p73α.

Among p53 family members, the NF-κB-mediated reduction was highly specific to p73α. The protein stability of p53, p73β and p63α was unaffected by the enforced expression of NF-κB. Lee and La Thangue (1999) described that p73β is much more stable than p73α, suggesting that the unique COOH-terminal extension of p73α is critical for its stability. Recently, we found that RanBPM binds to the extreme COOH-terminal region of p73α to inhibit its ubiquitination and thereby increasing its stability (Kramer *et al.*, 2005). However, RanBPM had undetectable effects on the stability of p53. Thus, it is possible that RanBPM might mask the p73α COOH-terminal lysine residues, which could be sites for ubiquitin ligation. Alternatively, the unique p73α COOH-terminal region could mediate the interaction with unknown cellular protein(s) required for the degradation of p73 induced by NF-κB. Of note, Wan and DeGregori (2003) found that NF-κB promotes T-cell survival by inhibiting the activation of p73 in response to antigenic stimulation. They described that NF-κB directly antagonizes the E2F-1-dependent upregulation of *p73* transcription. The interpretation that NF-κB inhibits the transcription of *p73* is contradicted by our present findings. In addition to the DNA-damage-induced stabilization of p73, p73 is regulated at mRNA level in response to certain apoptotic and differentiation stimuli. For example, p73 is transcriptionally induced by E2F-1 during the apoptotic response to T-cell receptor activation (Lissy *et al.*, 2000). Fontemaggi *et al.* (2001) found that *p73* mRNA is upregulated by E2F-1 during muscle, neuronal and monocytic differentiation. Therefore, it appears that employment of the NF-κB-dependent transcriptional or post-translational mechanism to downregulate p73 is dependent upon the types of stimulation and/or cell types. The propensity of cells to survive or die is determined by the balance between proapoptotic and prosurvival signals. In this connection, NF-κB-mediated degradation of p73 is a novel mechanism that regulates cell survival and death in response to a variety of cellular stresses.

Materials and methods

Cell culture and transfection

MEFs, and COS7 cells were grown in Dulbecco's modified Eagle's medium supplemented with 10% heat-inactivated fetal bovine serum (Invitrogen, Grand Island, NY, USA), 100 IU/ml penicillin and 100 μg/ml streptomycin. p53-deficient human lung carcinoma H1299 cells were cultured in RPMI 1640 medium supplemented with 10% heat-inactivated fetal bovine serum and antibiotic mixture. Cultures were maintained at 37°C in a water-saturated atmosphere of 5% CO_2 in air. For transfection, H1299 and COS7 cells were transfected with the indicated combinations of the expression plasmids using LipofectAMINE 2000 (Invitrogen) and FuGENE6 (Roche Molecular Biochemicals, Indianapolis, IN, USA), respectively.

Construction of the deletion mutant of p65

p65ΔC was generated by PCR-based strategy using the forward primer 5′-TAGAATTCGGGACGATCTGTTTCCC CTCATC-3′ and the reverse primer 5′-TTCTCGAGTTAAA GGACTGGGGCAGAGGACGG-3′. Underlined nucleotides were *Eco*RI and *Xho*I restriction sites. Amplified fragments were digested with *Eco*RI and *Xho*I, and subcloned into the identical restriction sites of pCMV-HA expression plasmid (Clontech Laboratories, Palo Alto, CA, USA) to give pCMV-HA-p65ΔC.

Immunoblotting

Cells were washed twice with phosphate-buffered saline (PBS), lysed in buffer containing 25 mM Tris-Cl, pH 8.0, 137 mM NaCl, 2.7 mM KCl, 1% Triton X-100 and protease inhibitor cocktail (Sigma Chemical Co., St Louis, MO, USA), and sonicated for 10 s followed by centrifugation at 15 000 r.p.m. for 10 min at 4°C to remove insoluble materials. Aliquots of whole-cell lysates (25–50 μg) were boiled in the SDS-sample buffer for 5 min, loaded onto 8% SDS–PAGE, and electrotransferred onto Immobilon-P membranes (Millipore, Bedford, MA, USA). The membranes were blocked with TBS-T (50 mM Tris-Cl, pH 8.0, 100 mM NaCl and 0.1% Tween-20) containing 5% nonfat dry milk, and then incubated at room temperature for 1 h with the monoclonal anti-FLAG (M2, Sigma Chemical Co.), monoclonal anti-HA (12CA5, Roche Molecular Biochemicals), monoclonal anti-p73 (Ab-4, NeoMarkers, Inc., Fremont, CA, USA), monoclonal anti-p53 (PAb1801, Santa Cruz Biotechnologies, Santa Cruz, CA, USA), monoclonal anti-p63 (Ab-1, NeoMarkers), polyclonal anti-p65 (C-20, Santa Cruz Biotechnologies), polyclonal anti-p50 (H-119, Santa Cruz Biotechnologies), or with polyclonal anti-actin (20–33, Sigma Chemical Co.) antibody, followed by an incubation with corresponding horseradish peroxidase-conjugated goat anti-mouse or anti-rabbit secondary antibody (Cell Signaling, Beverly, MA, USA) for 1 h at room temperature. Protein bands were finally detected by enhanced chemiluminescence detection system (Amersham Biosciences, Inc., Piscataway, NJ, USA).

Co-immunoprecipitation analysis
Equal amounts of whole-cell lysates were precleared with 30 μl of protein G-Sepharose (Amersham Bioscience). After centrifugation, the supernatant was incubated with the indicated antibodies at 4°C for 2 h. The immunocomplexes were then incubated with protein G-Sepharose beads at 4°C for 1 h, which were then pelleted by centrifugation at 15 000 r.p.m. for 5 min. The immunocomplexes were washed with the lysis buffer three times at 4°C, denatured with an equal volume of 2 × SDS-sample buffer, and analysed by immunoblotting with the desired primary antibodies.

RT–PCR
Total RNA was prepared by using RNeasy Mini Kit (Qiagen Inc., Valencia, CA, USA) according to the manufacturer's protocol. One microgram of total RNA was used to synthesize the first strand cDNA using random primers and a SuperScript II reverse transcriptase (Invitrogen). Reverse transcription was performed at 42°C for 1 h, and the reverse transcripts were amplified by standard PCR with rTaq DNA polymerase (Takara, Ohtsu, Japan). The primers used for PCR were as follows: *BAX*, 5′-TTTGCTTCAGGGTTTCATCC-3′ (sense) and 5′-CAGTTGAAGTTGCCGTCAGA-3′ (antisense); *GAPDH*, 5′-ACCTGACCTGCCGTCTAGAA-3′ (sense) and 5′-TCCACCACCCTGTTGCTGTA-3′ (antisense); *p73α*, 5′-TGGAACCAGACAGCACCTACTTCG-3′ (sense) and 5′-TGCTGGAAAGTGACCTCAAAGTGG-3′ (antisense).

Subcellular fractionation
Cells were washed twice with PBS, lysed in lysis buffer containing 10 mM Tris-HCl, pH 7.5, 1 mM EDTA, 0.5% Nonidet P-40, and protease inhibitor cocktail for 10 min at 4°C, and centrifuged at 3000 r.p.m. for 5 min at 4°C to separate the soluble (cytoplasmic) from the insoluble (nuclear) fraction. The insoluble fraction was washed completely with the lysis buffer and resuspended in buffer containing 25 mM Tris-Cl, pH 8.0, 137 mM NaCl, 2.7 mM KCl, 1% Triton X-100 and protease inhibitor cocktail. The nuclear and cytoplasmic fractions were then analysed by immunoblotting with monoclonal anti-Lamin B (Ab-1, Oncogene Reseach Products), or with monoclonal anti-α-tubulin antibody (Ab-2, NeoMarkers, Inc.).

Indirect immunofluorescence assay
H1299 cells were seeded onto the glass coverslips, and treated with TNF-α (20 ng/ml) or left untreated for 1 h cells were then fixed with 3.7% formaldehyde for 30 min at room temperature, and permeabilized with 0.2% Triton X-100 for 5 min at room temperature. After cells were blocked with 3% bovine serum albumin (BSA) for 1 h at room temperature, they were incubated with the polyclonal anti-p65 or with the polyclonal anti-p50 antibody for 1 h at room temperature. The primary antibodies were detected with FITC-conjugated secondary antibody (Invitrogen) for 1 h at room temperature. Cell nuclei were stained with 4′6-diamino-2-phenylindole (DAPI) (Sigma Chemical Co.), and cells were observed under a Fluoview laser scanning confocal microscope (Olympus, Tokyo, Japan).

Luciferase reporter assay
H1299 cells were co-transfected with 100 ng of the p53/p73-responsive luciferase reporter plasmid (*BAX* or *MDM2*), 10 ng of pRL-TK *Renilla* luciferase cDNA, and 25 ng of the expression plasmid for FLAG-p73α or FLAG-p53 together with or without the increasing amounts of HA-p65 and HA-p50 expression plasmids. At 48 h after transfection, cells were washed with PBS, and resuspended in passive lysis buffer (Promega Corp., Madison, WI, USA). Both firefly and *Renilla* luciferase activities were assayed with the dual-luciferase reporter assay system (Promega Corp.). The firefly luminescence signal was normalized based on the Renilla luminescence signal.

Protein decay rate analysis
COS7 cells were co-transfected with the indicated combinations of the expression plasmids. At 24 h after transfection, cells were treated with cycloheximide (Sigma Chemical Co.) at a final concentration of 100 μg/ml. At the indicated time points after the treatment with cycloheximide, cells were harvested, and whole-cell lysates were processed for immunoblot analysis with the anti-p73 or with the anti-actin antibody. Densitometry was used to quantify the amounts of FLAG-p73α which normalized to actin.

Ubiquitination assay
COS7 cells were co-transfected with the constant amount of FLAG-p73α and His-tagged ubiquitin, together with or without the increasing amounts of HA-p65 and HA-p50. At 48 h after transfection, cells were exposed to MG-132 (20 μM) for 6 h. Cells were then lysed in lysis buffer containing 6 M guanidine–HCl, 0.1 M Na_2HPO_4/NaH_2PO_4, pH 8.0 and 10 mM imidazole. Ubiquitinated materials were recovered by Ni^{2+}-NTA-agarose beads (Qiagen), and subsequently analysed by immunoblotting with the anti-p73 antibody.

FACS analysis
H1299 cells were co-transfected with indicated combinations of the expression plasmids. At 48 h after transfection, cells were washed twice with PBS, resuspended in 600 μl of a propidium iodide mixture containing 0.05% RNase, 0.25% Triton X-100 and 50 μg/ml of propidium iodide, and then incubated in the dark at 4°C for 30 min. Prior to performing FACS analysis, cells were filtered through a 40-μm nylon mesh. Cells were then analysed using the FACScan system (Becton Dickinson, Mountain View, CA, USA) in conjunction with CellQuest software (Becton Dickinson).

Colony formation assay
H1299 cells were co-transfected with indicated combinations of the expression plasmids. Total amount of plasmid DNA was kept constant (1 μg) with the empty plasmid. At 24 h after transfection, cells were selected with G418 (400 μg/ml) for 2 weeks. G418-resistant colonies were fixed in methanol, and stained with Giemsa's solution.

Abbreviations

CHX, cycloheximide; MEF, mouse embryonic fibroblasts; NF-κB, nuclear factor kappa B; TNF-α, tumor necrosis factor α; Ub, ubiquitin.

Acknowledgements

We thank members of our laboratory for helpful discussions. We also thank Y Nakamura for excellent technical assistance. We give special thanks to Dr M Karin for providing us with $p65^{-/-}$ MEF. This work was supported in part by a Grant-in-Aid from the Ministry of Health, Labour and Welfare for Third Term Comprehensive Control Research for Cancer, a Grant-in-Aid for Scientific Research on Priority Areas from the Ministry of Education, Culture, Sports, Science and Technology, Japan, and a Grant-in-Aid for Scientific Research from Japan Society for the Promotion of Science.

References

Agami R, Blandino G, Oren M, Shaul Y. (1999). *Nature* **399**: 809–813.
Balint E, Bates S, Vousden KH. (1999). *Oncogene* **18**: 3923–3929.
Bayon Y, Ortiz MA, Lopez-hernandez FJ, Gao F, Karin M, Pfahl M *et al.* (2003). *Mol Cell Biol* **23**: 1061–1074.
Beg AA, Baltimore D. (1996). *Science* **274**: 782–784.
Beg AA, Sha WC, Bronson RT, Baltimore D. (1995). *Nature* **376**: 167–170.
Bernassola F, Salomoni P, Oberst A, Di Como CJ, Pagano M, Melino G *et al.* (2004). *J Exp Med* **199**: 1545–1557.
Bourdon JC, Fernandes K, Murray-Zmijewski F, Liu G, Diot A, Xirodimas DP *et al.* (2005). *Genes Dev* **19**: 2122–2137.
Chang L, Kamata H, Solinas G, Luo JL, Maeda S, Venuprasad K *et al.* (2006). *Cell* **124**: 601–613.
Flores ER, Tsai KY, Crowley D, Sengupta S, Yang A, McKeon F *et al.* (2002). *Nature* **416**: 560–564.
Fontemaggi G, Gurtner A, Strano S, Higashi Y, Sacchi A, Piaggio G *et al.* (2001). *Mol Cell Biol* **21**: 8461–8470.
Gong J, Costanzo A, Yang HQ, Melino G, Kaelin Jr WG, Levrero M *et al.* (1999). *Nature* **399**: 806–809.
Gressner O, Schilling T, Lorenz K, Schulze Schleithoff E, Koch A, Schulze-Bergkamen H *et al.* (2005). *EMBO J* **24**: 2458–2471.
Grob TJ, Novak U, Maisse C, Barcaroli D, Luthi AU, Pirnia F *et al.* (2001). *Cell Death Differ* **8**: 1213–1223.
Huang TT, Wuerzberger-Davis SM, Seufzer BJ, Shumway SD, Kurama T, Boothman DA *et al.* (2000). *J Biol Chem* **275**: 9501–9509.
Ikawa S, Nakagawara A, Ikawa Y. (1999). *Cell Death Differ* **6**: 1154–1161.
Irwin MS, Kondo K, Marin MC, Cheng LS, Hahn WC, Kaelin Jr WG. (2003). *Cancer Cell* **3**: 403–410.
Jost CA, Marin MC, Kaelin Jr WG. (1997). *Nature* **389**: 191–194.
Kaghad M, Bonnet H, Yang A, Creancier L, Biscan JC, Valent A *et al.* (1997). *Cell* **90**: 809–819.
Kawai H, Nie L, Yuan ZM. (2002). *Mol Cell Biol* **22**: 6079–6088.
Kharbanda S, Ren R, Pandey P, Shafman TD, Feller SM, Weichselbaum RR *et al.* (1995). *Nature* **376**: 785–788.
Kim JS, Lee JM, Chwae YJ, Kim YH, Lee JH, Kim K *et al.* (2004). *Biochem Pharmacol* **67**: 1459–1468.
Kramer S, Ozaki T, Miyazaki K, Kato C, Hanamoto T, Nakagawara A. (2005). *Oncogene* **24**: 938–944.
Lee CW, La Thangue NB. (1999). *Oncogene* **18**: 4171–4181.
Leng RP, Lin Y, Ma W, Wu H, Lemmers B, Chung S *et al.* (2003). *Cell* **112**: 779–791.
Lissy NA, Davis PK, Irwin M, Kaelin Jr WG, Dowdy SF. (2000). *Nature* **407**: 642–645.
Mantovani F, Piazza S, Gostissa M, Strano S, Zacchi P, Mantovani R *et al.* (2004). *Mol Cell* **14**: 625–636.
Melino G, De Laurenzi V, Vousden KH. (2002). *Nat Rev Cancer* **2**: 605–615.
Muta T, Takeshige K. (2001). *Eur J Biochem* **268**: 4580–4589.
Nakagawa T, Takahashi M, Ozaki T, Watanabe K, Todo S, Mizuguchi H *et al.* (2002). *Mol Cell Biol* **22**: 2575–2585.
Pozniak CD, Radinovic S, Yang A, McKeon F, Kaplan DR, Miller FD. (2000). *Science* **289**: 304–306.
Rossi M, De Laurenzi V, Munarriz E, Green DR, Liu YC, Vousden KH *et al.* (2005). *EMBO J* **24**: 836–848.
Stiewe T, Putzer BM. (2002). *Cell Death Differ* **9**: 237–245.
Stiewe T, Zimmermann S, Frilling A, Esche H, Putzer BM. (2002). *Cancer Res* **62**: 3598–3602.
Strano S, Monti O, Pediconi N, Baccarini A, Fontemaggi G, Lapi E *et al.* (2005). *Mol Cell* **18**: 447–459.
Van Antwerp DJ, Martin SJ, Kafri T, Green DR, Verma IM. (1996). *Science* **274**: 787–789.
Wan YY, DeGregori J. (2003). *Immunity* **18**: 331–342.
Wang CY, Mayo MW, Baldwin ASJ. (1996). *Science* **274**: 784–787.
Wang CY, Mayo MW, Korneluk RG, Goeddel DV, Baldwin SJ. (1998). *Science* **281**: 1680–1683.
Yamagishi N, Miyakoshi J, Takebe H. (1997). *Int J Radiat Biol* **72**: 157–162.
Yang A, Kaghad M, Wang Y, Gillett E, Fleming MD, Dotsch V *et al.* (1998). *Mol Cell* **2**: 305–316.
Yang A, McKeon F. (2000). *Nat Rev Mol Cell Biol* **1**: 199–207.
Yang A, Walker N, Bronson R, Kaghad M, Oosterwegel M, Bonnin J *et al.* (2000). *Nature* **404**: 99–103.
Yuan ZM, Shioya H, Ishiko T, Sun X, Gu J, Huang YY *et al.* (1999). *Nature* **399**: 814–817.
Zaika AI, Slade N, Erster SH, Sansome C, Joseph TW, Pearl M *et al.* (2002). *J Exp Med* **196**: 765–780.
Zeng X, Chen L, Jost CA, Maya R, Keller D, Wang X *et al.* (1999). *Mol Cell Biol* **19**: 3257–3266.

Supplementary Information accompanies the paper on the Oncogene website (http://www.nature.com/onc).

Molecular Biology of the Cell
Vol. 17, 4888–4895, November 2006

Critical Role of PICT-1, a Tumor Suppressor Candidate, in Phosphatidylinositol 3,4,5-Trisphosphate Signals and Tumorigenic Transformation[D]

Fumiaki Okahara,*†‡ Kouichi Itoh,§ Akira Nakagawara,‖ Makoto Murakami,*¶ Yasunori Kanaho,† and Tomohiko Maehama*‡

*Biomembrane Signaling Project, Tokyo Metropolitan Institute of Medical Science, Tokyo 113-8613, Japan; †Department of Physiological Chemistry, Graduate School of Comprehensive Human Sciences and Institute of Basic Medical Sciences, University of Tsukuba, Tsukuba 305-8575, Japan; §Laboratory of Molecular Pharmacology, Department of Pharmaceutical Technology, Faculty of Pharmaceutical Sciences at Kagawa Campus, Tokushima Bunri University, Kagawa 769-2193, Japan; ‖Division of Biochemistry, Chiba Cancer Center Research Institute, Chiba 260-8717, Japan; and ¶PRESTO, Japan Science and Technology Corporation, Saitama 332-0012, Japan

Submitted April 12, 2006; Revised August 10, 2006; Accepted August 31, 2006
Monitoring Editor: John York

The tumor suppressor phosphatase and tensin homolog deleted on chromosome 10 (PTEN) regulates diverse cellular functions by dephosphorylating the lipid second messenger, phosphatidylinositol 3,4,5-trisphosphate (PIP_3). Recent study revealed that PICT-1/GLTSCR2 bound to and stabilized PTEN protein in cells, implicating its roles in PTEN-governed PIP_3 signals. In this study, we demonstrate that RNA interference-mediated knockdown of PICT-1 in HeLa cells down-regulated endogenous PTEN and resulted in the activation of PIP_3 downstream effectors, such as protein kinase B/Akt. Furthermore, the PICT-1 knockdown promoted HeLa cell proliferation; however the proliferation of PTEN-null cells was not altered by the PICT-1 knockdown, suggesting its dependency on PTEN status. In addition, apoptosis of HeLa cells induced by staurosporine or serum-depletion was alleviated by the PICT-1 knockdown in the similar PTEN-dependent manner. Most strikingly, the PICT-1 knockdown in HeLa and NIH3T3 cells promoted anchorage-independent growth, a hallmark of tumorigenic transformation. Furthermore, PICT-1 was aberrantly expressed in 18 (41%) of 44 human neuroblastoma specimens, and the PICT-1 loss was associated with reduced PTEN protein expression in spite of the existence of PTEN mRNA. Collectively, these results suggest that PICT-1 plays a role in PIP_3 signals through controlling PTEN protein stability and the impairment in the PICT-1–PTEN regulatory unit may become a causative factor in human tumor(s).

INTRODUCTION

Phosphoinositide 3-kinase (PI3K) plays pivotal roles in regulating cell proliferation and apoptosis by producing the lipid second messenger phosphatidylinositol 3,4,5-trisphosphate (PIP_3), in response to various stimuli (Cantley, 2002). The resulting PIP_3 lipid product activates diverse signaling pathways by recruiting its downstream effector proteins to the plasma membrane through its binding to specific protein domains, such as pleckstrin homology domain (Lemmon and Ferguson, 2000; Vanhaesebroeck *et al.*, 2001). The tumor suppressor phosphatase and tensin homolog deleted on chromosome 10 (PTEN) dephosphorylates PIP_3 to negatively regulate PI3K/PIP_3 signals (Maehama and Dixon, 1998; Myers *et al.*, 1998; Cantley and Neel, 1999); therefore, PTEN inactivation results in the hyperactivation of PIP_3 downstream signals and provides enormous impact on diverse cellular functions, leading to tumorigenesis (Di Cristofano and Pandolfi, 2000; Leslie and Downes, 2004). Moreover, inactivation of PTEN has been found associated with the hyperactivation of PIP_3 downstream signals in a variety of human tumors, including glioblastoma and endometrial carcinoma (Ali *et al.*, 1999). Because accumulating body of evidence unequivocally indicates the biological significance of PTEN and its relevance to tumorigenesis, it has been speculated that the impairment in the regulatory system for PTEN function may influence PTEN-governed cellular functions and become potential causative factor in tumorigenesis. In support of this notion, recent studies have revealed that several PTEN-binding proteins and kinases that directly phosphorylate PTEN regulate PTEN protein stability, enzymatic activity, and localization in cells (Vazquez *et al.*, 2000; Wu *et al.*, 2000a, b; Vazquez *et al.*, 2001; Miller *et al.*, 2002; Das *et al.*, 2003; Lu *et al.*, 2003; Sumitomo *et al.*, 2004; Li *et al.*, 2005; Valiente *et al.*, 2005); however, their contribution to tumorigenesis remains elusive.

This article was published online ahead of print in *MBC in Press* (http://www.molbiolcell.org/cgi/doi/10.1091/mbc.E06-04-0301) on September 13, 2006.

[D] The online version of this article contains supplemental material at *MBC Online* (http://www.molbiolcell.org).

‡ Present address: Department of Biochemistry and Cell Biology, National Institute of Infectious Diseases, 1-23-1 Toyama, Shinjuku-ku, Tokyo 162-8640, Japan.

Address correspondence to: Tomohiko Maehama (tmaehama@nih.go.jp).

Protein interacting with the carboxy terminus-1/glioma tumor suppressor candidate region 2 (*PICT-1/GLTSCR2*) gene was originally identified as a candidate tumor suppressor gene located at human chromosome 19q13.32 (Smith *et al.*, 2000b). Although several groups have proven that the 19q13.32 locus is frequently altered in a variety of human tumors, a tumor suppressor gene(s) specifically encoded in this region has yet to be identified (Smith *et al.*, 2000a, b; Mora *et al.*, 2001; Hartmann *et al.*, 2002). We recently unveiled that PICT-1 was able to bind to PTEN and was required for maintaining PTEN protein stability in cells (Okahara *et al.*, 2004). PICT-1 inactivation induced by RNA interference (RNAi) renders PTEN protein unstable and leads to a rapid degradation of PTEN in cells (Okahara *et al.*, 2004). These observations raise the possibility that a loss of PICT-1 function may induce the activation of PI3K/PIP_3-mediated signals through the inactivation of PTEN, implicating that PICT-1 may function as the tumor suppressor locating at 19q13.32 locus. In this study, we demonstrated that the PICT-1 inactivation promoted both anchorage-dependent and anchorage-independent cell proliferation through the activation of PIP_3 downstream effectors. Moreover, the expression of PICT-1 was impaired with significant frequency in human neuroblastoma, in which PTEN down-regulation was associated with impaired PICT-1 expression. Our findings provide insight into an intimate link between impaired PTEN regulation and human tumor(s).

MATERIALS AND METHODS

RNA Interference Constructs

Twenty-one- or 23-nucleotide small interfering RNAs (siRNAs) with UU overhangs at both 3′ ends were prepared as described previously (Yu *et al.*, 2002). Target sequences of PIC247, PIC749, and PT1084 siRNAs corresponded to nucleotides 247–267 and 749–769 of human PICT-1/GLTSCR2 (GenBank accession no. AF182076) and nucleotides 1084–1106 of human PTEN (GenBank accession no. U92436), respectively. GFP5 control siRNA was described previously (Yu *et al.*, 2002). For the construction of a gene silencing vector for human PTEN (PTEN/pSilencer), oligo DNA encoding short hairpin RNA that shares core target sequence with PT1084 siRNA was cloned into pSilencer 3.1-H1 hygro vector (Ambion, Austin, TX) according to the manufacturer's protocol. A gene silencing vector for PICT-1/GLTSCR2 (GLT318SH/pSilencer) was described previously (Okahara *et al.*, 2005). For the construction of gene silencing vectors for mouse Pict-1, Pic675/pSilencer, and Pic1343/pSilencer, oligo DNAs encoding short hairpin RNAs that target nucleotides 675–695 and nucleotides 1343–1363 of mouse Pict-1 (GenBank accession no. NM_133831), respectively, were cloned into pSilencer 3.1-H1 hygro vector.

Cell Culture and Transfections

HeLa cervical carcinoma cells and U87MG glioblastoma cells were maintained at 37°C with 5% CO_2 in DMEM supplemented with 5% fetal bovine serum, 50 U/ml penicillin, and 50 μg/ml streptomycin. Transfections of cells cultured on ø35-mm dish (1.6–2.0 × 10^5 cells) were performed using RNAiFect (QIAGEN, Valencia, CA) or FuGENE6 (Roche Diagnostics, Indianapolis, IN) according to the manufacturers' protocol. Either RNAiFect (9 μl) with 2 μg of siRNA or FuGENE6 (3 μl) with 2.5 μg of plasmid DNA was used for each transfection. NIH3T3 cells were maintained at 37°C with 5% CO_2 in DMEM supplemented with 10% calf serum, 50 U/ml penicillin, and 50 μg/ml streptomycin. Lipofectamine 2000 (Invitrogen) was used for the transfection of NIH3T3 cells according to the protocol deposited on manufacturer's Web site (www.invitrogen.com).

Immunoblots

To prepare samples for immunoblot analyses, cells/proteins were precipitated in 10% trichloroacetic acid; then, precipitates were collected, washed, and dissolved in the solubilizing solution consisting of 9 M urea, 2% Nonidet-P40, and 65 mM dithiothreitol. After the determination of protein concentration, SDS, bromophenol blue, and Tris base were added to the lysate to 2.5%, 0.1%, and 20 mM, respectively. Immunoblots were conducted as described previously (Okahara *et al.*, 2004, 2005). Antibodies used were anti-PICT-1/GLTSCR2 (Okahara *et al.*, 2005), anti-PTEN (Cascade Bioscience, Winchester, MA), anti-actin (Sigma-Aldrich, St. Louis, MO), anti-phospho-Akt [S473] (Cell Signaling Technology, Beverly, MA), anti-Akt1/2 (Santa Cruz Biotechnology, Santa Cruz, CA), anti-phospho-glycogen synthase kinase (GSK)3β [S9] (Cell Signaling Technology), anti-phospho-p70 S6 kinase (S6K) [T389] (Cell Signaling Technology), anti-cleaved caspase-3 [D175] (Cell Signaling Technology), and anti-p70 S6K (Cell Signaling Technology). The relative intensity of immunoreactive bands was measured by NIH Image 1.62 (http://rsb.info.nih.gov/nih-image/). Typical images from repeated experiments are represented in each figure.

Proliferation Assay

After the transfection with pSilencer or PTEN/pSilencer, HeLa cells were cultured and expanded for 7–14 d in the presence of 300 μg/ml hygromycin B to enrich cells harboring the silencing constructs. These transformants or U87MG cells were further transfected with either PIC247 or GFP5 siRNA and then cultured for 3 d. Cells were trypsinized and seeded onto 96-well plates (1.0×10^4 cells/well) with serum-free medium, followed by the incubation for 4 h to allow cells settle onto the wells. Proliferation assay was conducted in sextuplicate by using Cell Proliferation Kit II (Roche Diagnostics) according to the manufacturer's protocol. Briefly, after the addition of chromogen solution, cells were incubated at 37°C for 2 h to allow color develops; then, absorbance at 450 and 655 nm was measured. Unpaired Student's *t* test was used to calculate statistical significance, and typical data from three independent experiments are represented.

Apoptosis Assay

HeLa cells transfected with siRNA (GFP5, PIC749, or PT1084) were cultured for 2 d, and then 2.0×10^4 cells were seeded onto a coverslip (ø15 mm). After the incubation for 8–12 h to allow cells settle onto the coverslip, the cells were treated with 1 μM staurosporine for 4 h, serum starved for 24 h, or left untreated. Apoptotic cells were evaluated by the terminal deoxynucleotidyl transferase-mediated dUTP nick-end labeling (TUNEL) method using Dead-End fluorometric system (Promega, Madison, WI) according to the manufacturer's protocol. Propidium iodide was used for the counterstaining and at least 500 cells were examined for each evaluation. Typical data from four independent experiments are represented.

Soft-Agar Assay

After the transfection with pSilencer or GLT318SH/pSilencer, HeLa cells were cultured and expanded for 7–14 d in the presence of 300 μg/ml hygromycin B. Then, the cells (2.0×10^5 cells) were suspended in 3 ml of top agar (DMEM containing 2% fetal bovine serum, 300 μg/ml hygromycin B, and 0.4% SeaPlaque GTG agarose [Cambrex Bio Science Walkersville, Walkersville, MD]) and added onto prelayered bottom agar (3 ml of DMEM containing 2% fetal bovine serum, 300 μg/ml hygromycin B, and 0.5% SeaPlaque GTG agarose) in a ø60-mm dish. For the NIH3T3 cells, cells were transfected with pSilencer, Pic675/pSilencer, or Pic1343/pSilencer, and then the same assay was performed except using hygromycin at 100 μg/ml, fetal bovine serum at 10%, bottom agar at 0.5%, and top agar at 0.4%. After the incubation at 37°C with 5% CO_2 for 16 d, the diameter of colonies was measured. Unpaired Student's *t* test was used to calculate statistical significance.

Human Neuroblastoma Specimens

All tumor samples were collected through institutional review board-approved protocol after obtaining informed consents. RNA samples from randomly selected 44 patients with neuroblastoma were transcribed into cDNA using Moloney murine leukemia virus reverse transcriptase (Toyobo Engineering, Osaka, Japan), followed by polymerase chain reaction (PCR) analyses. To prepare protein samples, sectioned frozen tumor specimens were homogenized in 10% trichloroacetic acid at 4°C; then, precipitates were dissolved and used for the immunoblot analyses as described above.

Polymerase Chain Reaction

To analyze the expression of PICT-1 and PTEN transcripts, PCR was conducted in a 10-μl reaction mixture by using 0.2 μg of cDNA as a template and PrimeSTAR polymerase (Takara, Kyoto, Japan). Primer sequences used for PTEN were CCTTTTGAAGACCATAACCCACC (forward) and ATCACCACACACAGGTAACGGC (reverse); for PICT-1, CATTCCAGGAGCTGTGCGA (forward) and GCGAGTCTCCGGCATCTG (reverse); for actin, GGAGAAAATCTGGCACCACACCT (forward) and AGGAAGGAAGGCTGGAAGAGTG (reverse); and for mouse Pict-1, AGGCGAAAGGAGGAGTTA (forward) and TTCTGCCTCTTTCTCACG (reverse).

RESULTS

PICT-1 Knockdown Activates PI3K/PIP_3 Signals

In the previous study, we demonstrated that PICT-1 stabilized PTEN protein in cells and a loss of PICT-1 rendered PTEN protein unstable, leading to a decrease in PTEN protein level in MCF7 breast carcinoma cells (Okahara *et al.*, 2004). Because PTEN constrains the PI3K/PIP_3 signaling,

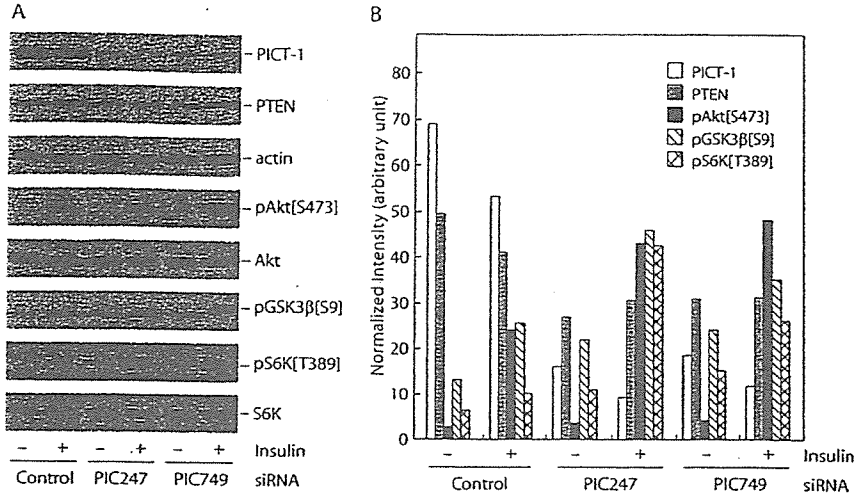

Figure 1. PICT-1 knockdown induces PTEN down-regulation and activation of PIP_3 downstream signals. HeLa cells were transfected with GFP5 siRNA (Control) or PICT-1–directed siRNAs (*PIC247* and *PIC749*) and cultured for 2 d. After the serum-starvation for 24 h, cells were stimulated with 0.5 μg/ml insulin for 3 min (±) or left untreated (−). Cell lysates were prepared and subjected to immunoblot analyses by indicated antibodies as described in *Materials and Methods*. (A) The band intensity of PICT-1, PTEN, pAkt[S473], pGSK3β [S9], and pS6K[T398] was measured by NIH Image 1.62. (B) Values normalized to that of actin are represented.

these observations raise the possibility that the PICT-1 loss activates PIP_3 downstream signals by virtue of the PTEN down-regulation. To explore this possibility, we knocked down PICT-1 in PICT-1– and PTEN-expressing cells and examined the effect of the knockdown on PI3K/PIP_3 signals. As shown in Figure 1, transfection of PICT-1-targeted siRNAs (PIC247 and PIC749) into HeLa cells induced robust reduction (79 and 75%, respectively) in PICT-1 protein levels. The residual PICT-1 protein observed in PIC247- and PIC749-treated samples is likely to be derived from cells into which siRNAs were not effectively delivered, because the transfection efficiency was ~70% under this condition (our unpublished data). Levels of PTEN protein were concomitantly decreased (36 and 32%, respectively) after the PICT-1 knockdown; this observation was comparable to our previous results observed in MCF7 cells (Okahara *et al.*, 2004). Insulin-induced phosphorylation of Akt at serine-473, which reflects the activation of the PIP_3 signal and is required for Akt kinase activity, was significantly enhanced in PICT-1-knocked down cells, compared with that in control cells (Figure 1). As well as the insulin-induced Akt phosphorylation, consequent phosphorylation of GSK3β at serine-9, a direct phosphorylation site for Akt, was also enhanced by the PICT-1 knockdown (Figure 1). Most strikingly, in PICT-1-knocked down cells, insulin stimulation induced robust phosphorylation of p70 S6K at threonine-389, a phosphorylation site for another Akt downstream kinase, mammalian target of rapamycin; whereas control cells displayed very small increase in the phosphorylation under this condition (Figure 1). These results clearly indicate PICT-1 plays a role in PI3K/PIP_3 signals and suggest that PICT-1 functions as a negative regulator for this signaling pathway.

PICT-1 Knockdown Promotes Cell Proliferation and Suppresses Apoptosis in PTEN-dependent Manner

Several studies have defined that a modulation of PI3K/PIP_3 signals primarily affects cell proliferation and apoptosis. Therefore, we next tested whether the proliferation would be influenced by the PICT-1 knockdown. HeLa cells were subjected to the RNAi for PICT-1, PTEN, or both simultaneously, and their proliferation was then monitored by colorimetric 2,3-bis(2-methoxy-4-nitro-5-sulfophenyl)-2*H*-tetrazolium-5-carboxanilide proliferation assay. Control cells (GFP5 siRNA-transfected cells) exhibited slow proliferation under low- and no-serum conditions (Figure 2; our unpublished data), and the proliferation was significantly promoted (1.7-fold at 48 h) by siRNA-mediated PICT-1 knockdown (Figure 2; our unpublished data). Similar enhancement in the proliferation was observed in all cases in which PICT-1 was knocked down by several different siRNAs (Supplemental Figure S1), excluding the possibility of "off-target" effect of PICT-1–targeted siRNAs. These results, together with the result that forced expression of PICT-1 suppressed HeLa cell proliferation (Supplemental Figure S2), suggest the critical role of PICT-1 in regulating cell proliferation. Knockdown of PTEN by the vector-based RNAi as well as siRNA-mediated RNAi (our unpublished data) in HeLa cells also promoted the proliferation; however, additional knockdown of PICT-1 over the PTEN-knocked down cells showed no further effect on the proliferation (Figure 2). Impact of the PICT-1 knockdown on HeLa cell proliferation thus seemed to depend on the existence of PTEN. As supporting evidence for this possibility, knockdown of PICT-1 in PTEN-null U87MG glioblastoma cells also exhibited no effect on their proliferation (Figure 2); reintroduction of PTEN in PTEN-null PC3 cells restored the effect of PICT-1 knockdown on cell proliferation (Supplemental Figure S3). We further tested several cell lines and observed same dependency of the PICT-1 effect onto the PTEN status (our unpublished data).

In addition to the effect on cell proliferation, the PICT-1 knockdown affected apoptosis in the similar PTEN-dependent manner. As shown in Figure 3, staurosporine, a protein kinase inhibitor, induced robust apoptotic cell death (3.3-fold increase) when evaluated by the TUNEL method, and serum depletion for 24 h also induced substantial increase (1.8-fold) in the apoptosis (Figure 3A). Cleavage of caspase-3, which indicated its activation, was also induced by staurosporine and serum depletion associated with increased apoptosis (Figure 3B). Knockdown of PICT-1 clearly suppressed both apoptosis and caspase-3 activation induced by staurosporine and serum depletion (Figure 3). It is of note that staurosporine treatment (4 h) also induced robust down-regulation of PICT-1 by unknown mechanism; however, 4-h incubation may not be enough to induce PTEN down-regulation even after complete disappearance of PICT-1 (Figure 3B). The PTEN knockdown also suppressed apoptosis and caspase-3 activation; however, combinational knockdown of PICT-1 and PTEN displayed no additional effect on the suppression, similar to their effects on cell proliferation (Figures 2 and 3). These observations collectively indicate that PICT-1 may be involved in cell prolifer-

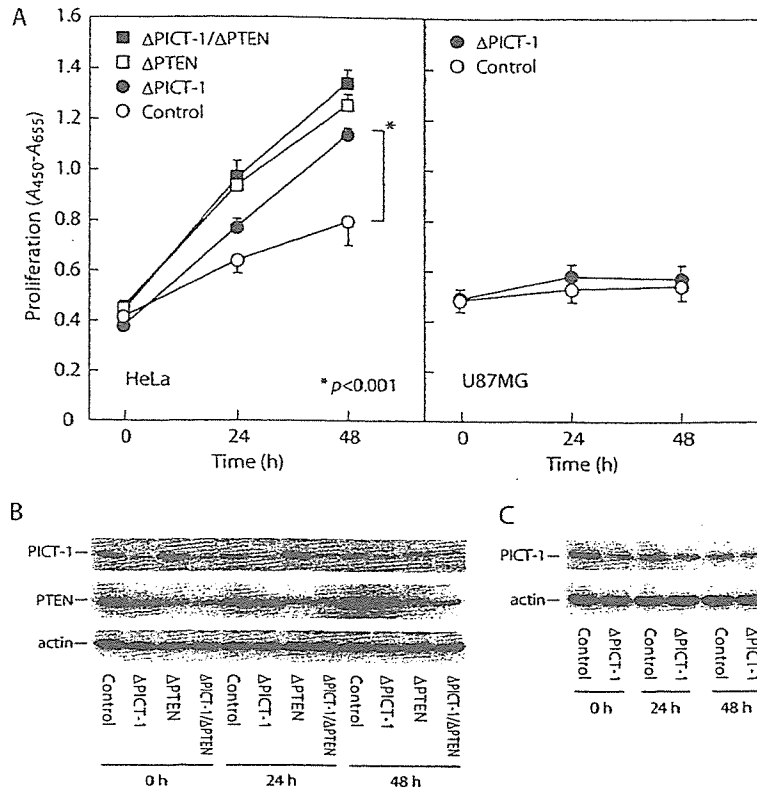

Figure 2. Effects of PICT-1 and PTEN knockdown on the proliferation of HeLa and U87MG cells. (A) HeLa cells (left) were transfected with pSilencer (circles; Control and ΔPICT-1) or PTEN/pSilencer (squares; ΔPTEN and ΔPICT-1/ΔPTEN) and cultured in the presence of hygromycin B. Cells harboring the gene silencing construct were further transfected with GFP5 siRNA for control knockdown (open symbols; Control and ΔPTEN) or PIC749 siRNA for PICT-1 knockdown (closed symbols; ΔPICT-1 and ΔPICT-1/ΔPTEN). The proliferation at indicated time was monitored as described in *Materials and Methods*. U87MG cells (right) were transfected with GFP5 (open circles; Control) or PIC247 (closed circles; ΔPICT-1) siRNAs and the proliferation was monitored. Mean ± SD from sextuplicated experiment is represented. HeLa cell lysates (B) and U87MG cell lysates (C) were prepared and subjected to immunoblot analyses by indicated antibodies as described in *Materials and Methods*.

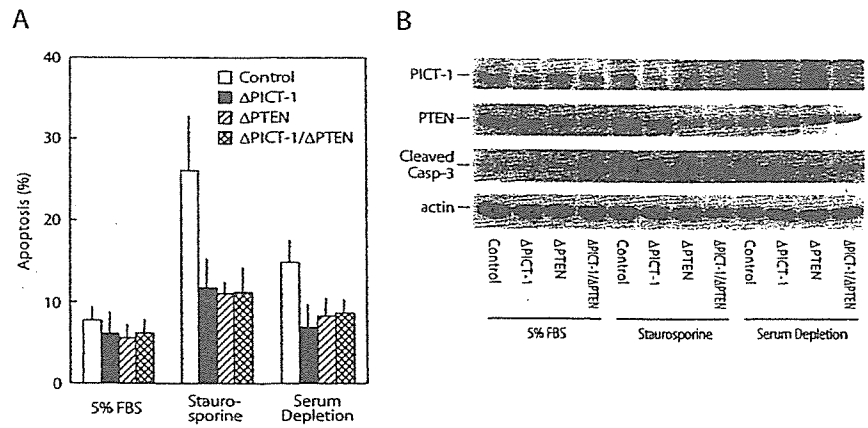

Figure 3. PICT-1 knockdown induces decreased susceptibility to apoptotic cell death. (A) HeLa cells were transfected with GFP5 (Control; open columns), PIC749 (ΔPICT-1; closed columns), PT1084 (ΔPTEN; hatched columns), or a combination of PIC749 and PT1084 (ΔPICT-1/ΔPTEN; cross-hatched columns) and cultured for 2 d. Cell were then transferred onto a coverslip and incubated in the presence of 5% serum or 1 μM staurosporine or in the absence of serum as indicated. Apoptosis was evaluated by the TUNEL method as described in *Materials and Methods*. All data represent mean ± SD. (B) Cell lysates were prepared and subjected to immunoblot analyses by indicated antibodies as described in *Materials and Methods*.

ation and survival signals and may function through regulating PTEN.

Tumorigenic Transformation by the PICT-1 Inactivation

Tumor cells usually display anchorage-independent growth, whereas nontransformed cells do not; therefore, this characteristic is commonly used as a criterion for tumorigenic transformation of cells. One question arising here is whether a loss of PICT-1 is responsible for the alteration in this characteristic, because PTEN, of which stability is regulated by PICT-1, is known to suppress the tumorigenic transformation. To address this question, we used colony formation assay to evaluate the effect of the PICT-1 knockdown on anchorage-independent growth. HeLa cells exhibited very slow growth under low-serum (2%) condition and only formed tiny colonies in the soft-agar (Figure 4A). To accomplish the knockdown of PICT-1 during 16-d culture, we transfected HeLa cells with PICT-1 short hairpin RNA-encoded vector (GLT318SH/pSilencer), which was previously shown to knock down PICT-1 effectively (Okahara *et al.*, 2005). Because the pSilencer vector contained hygromycin resistance gene, cells harboring the vector thereby grew in the soft-agar in the presence of hygromycin B. As shown in Figure 4, A and B, the GLT318SH/pSilencer-transfected cells conspicuously formed large colonies (average diameter 527 μm) in the soft-agar, whereas control vector-transfected cells barely formed small colonies (average diameter 349 μm). The number of colonies formed in the soft-agar was comparable in both control and PICT-1-knocked down cells, indicating comparable transfection efficiency. It is of note that the knockdown of PICT-1 in PTEN-positive MCF7 cells also promoted the colony formation in the soft-agar and the PTEN knockdown also increased colony formation activity (Supplemental Figure S4). We further tested the effect of

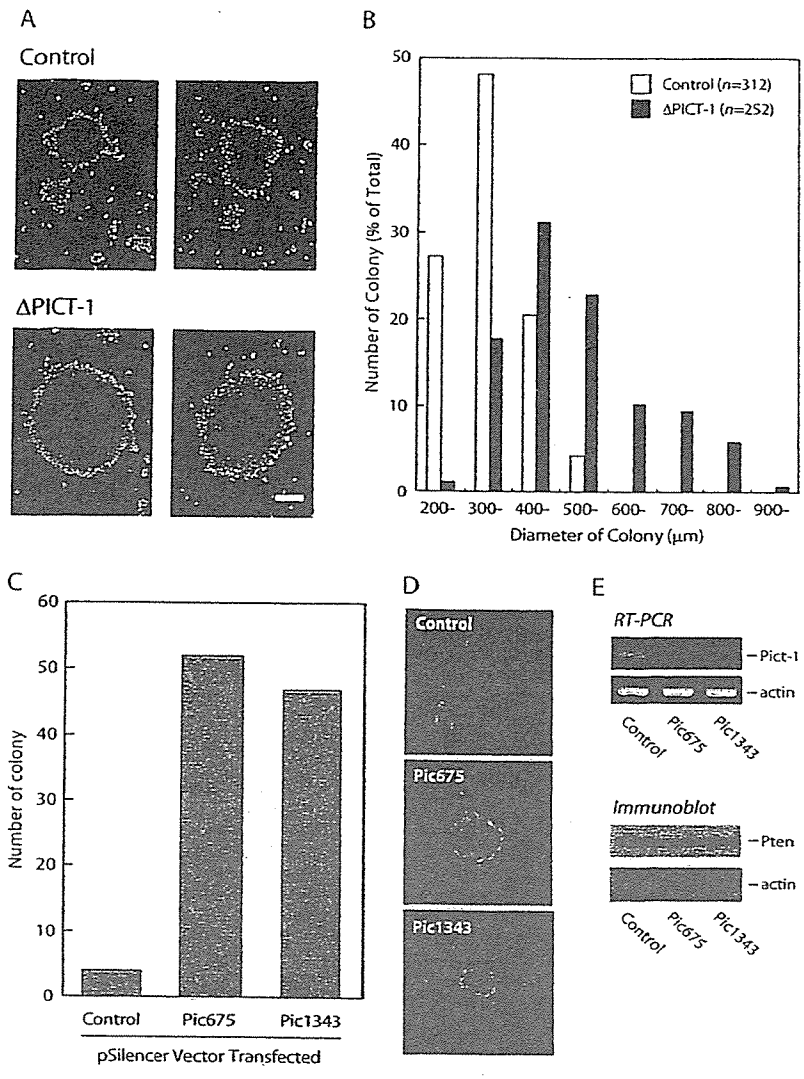

Figure 4. PICT-1 knockdown promotes anchorage-independent growth in soft-agar. (A and B) HeLa cells were transfected with pSilencer (Control) or GLT318SH/pSilencer (ΔPICT-1), and then colony formation in the soft-agar was assayed as described in *Materials and Methods*. (A) Typical images of formed colonies of control cells (Control; top) and ΔPICT-1 cells (ΔPICT-1; bottom). Bar, 200 μm. (B) Distribution of colony diameter from control cells (n = 312) and ΔPICT-1 cells (n = 252) is represented as a histogram. (C–E) NIH3T3 cells were transfected with pSilencer (Control), Pic675/pSilencer (Pic675), or Pic1343/pSilencer (Pic1343). (C) Number of colonies formed after 16-d culture was determined. Typical images of formed colony are represented in D. (E) Protein and RNA fractions were prepared from each transfectant and subjected to immunoblot analysis and reverse transcription (RT)-PCR to detect indicated protein and transcript, respectively.

PICT-1 knockdown on tumorigenic transformation in non-cancerous NIH3T3 cell (Figure 4, C–E). Knockdown of mouse Pict-1 by two different RNAi constructs (Pic675/pSilencer and Pic1343/pSilencer) strikingly promoted colony formation in the soft-agar, whereas control cells formed few very tiny colonies under this condition (Figure 4, C–E). Although we cannot conclude that PICT-1 functions as a critical tumor suppressor solely from these observations, it is pronounced that PICT-1 exerts its effect on tumorigenic transformation in vitro.

Impaired PICT-1 Function in Human Neuroblastoma

The aforementioned in vitro effects of the PICT-1 knockdown give rise to the possibility that a loss of PICT-1 function participates in the genesis of tumors and/or tumor progression through the PTEN down-regulation. In support of this notion, genetic studies have indeed demonstrated that human chromosome 19q13.32 locus where PICT-1 gene locates was frequently altered in a variety of human tumors, including low-grade glioma and neuroblastoma (Smith *et al.*, 2000a, b; Mora *et al.*, 2001; Hartmann *et al.*, 2002). Therefore, we next asked whether the PTEN down-regulation would be associated with impaired PICT-1 expression in human tumors. To address this question, we first analyzed expression levels of PICT-1 and PTEN proteins and their correlation in human neuroblastoma specimens (Figure 5, A and B). Among seven specimens we tested, three specimens (4–6) displayed nearly complete loss of PTEN protein expression (Figure 5); although these specimens retained PTEN mRNA expression to an extent similar to others (Figure 5, C and D). Immunoblot and RT-PCR analyses revealed that these specimens showed lower PICT-1 protein/mRNA expression compared with the others. Furthermore, expression levels of PICT-1 and PTEN proteins from seven specimens exhibited significant correlation (r = 0.691) (Figure 5B). These results suggest that PICT-1 regulates PTEN protein levels and that PICT-1 inactivation leads to the PTEN down-regulation in vivo, reflecting the in vitro observations (Figure 1 and Okahara *et al.*, 2004).

We further analyzed the expression of PICT-1 transcript by using RNA samples from randomly selected 44 neuroblastomas, including 17 stage 1 tumors, seven stage 2 tumors, four stage 3 tumors, and 14 stage 4a/4s tumors; tumor stage of others was not defined/confirmed (see Supplemental Table S1 for details). As expected, these tissues showed aberrant expression of PICT-1 (loss of expression or altered splicing) with significant frequency (Figure 6); six in stage 1 tumors (35%), two in stage 2 tumors (29%), two in stage 3

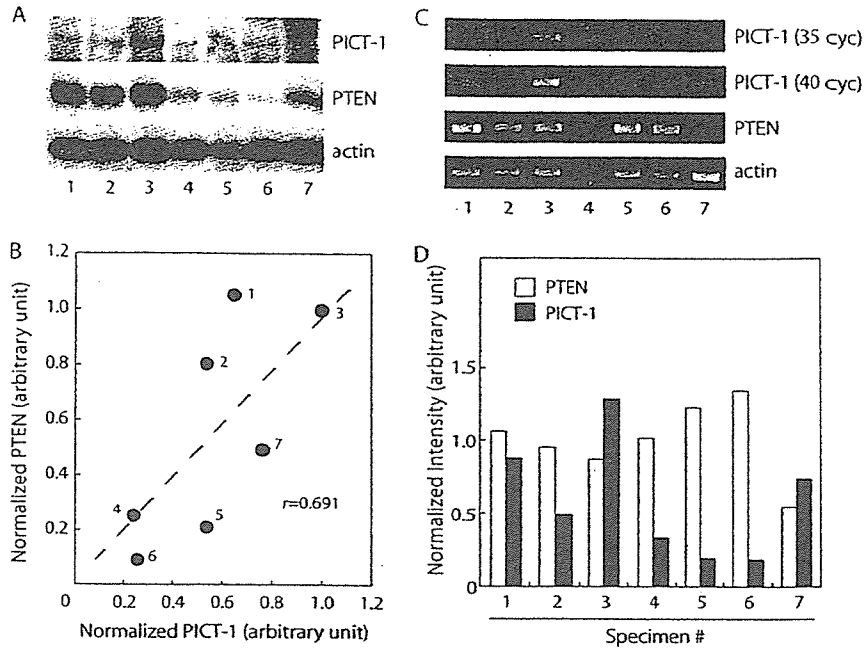

Figure 5. Expression of PICT-1 and PTEN in human neuroblastomas. Protein and RNA fractions were prepared from seven human neuroblastoma specimens (1–7) and subjected to immunoblot analysis (A and B) and RT-PCR (C and D), respectively. (A) For the immunoblot analysis, 20 μg of proteins for each sample was used to detect PICT-1 and PTEN protein expression. (B) The relative intensity of immunoreactive bands was measured by NIH Image 1.62, and normalized values of PICT-1 and PTEN proteins (to actin) are plotted. Pearson r (r = 0.691) is represented in the plot. (C) Expression of PICT-1, PTEN, and actin transcripts was analyzed by RT-PCR as described in *Materials and Methods*. (D) Signal intensity of PCR products was measured by NIH Image 1.62, and values normalized to that of actin are represented.

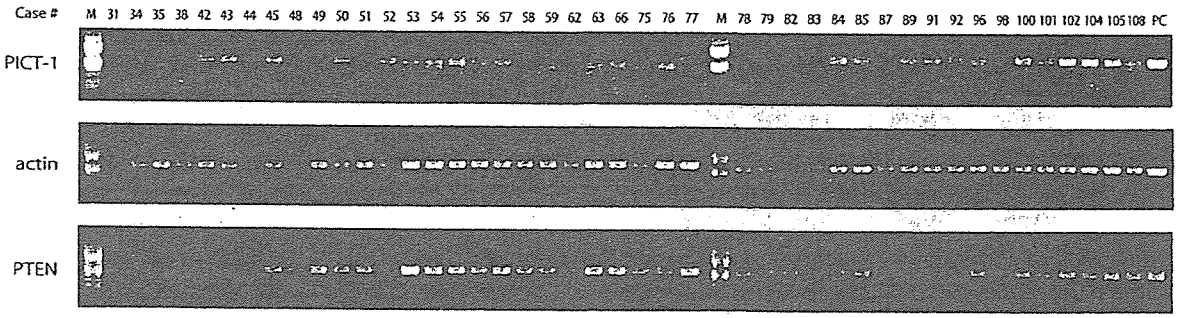

Figure 6. Aberrant expression of PICT-1 transcript in human neuroblastomas. PCR analyses were performed to detect PICT-1 (top) and PTEN (middle) transcript levels in human neuroblastoma samples. Actin expression (bottom) was used as an internal control. RNA from MCF7 cells was used as a positive control (PC). M, standard size marker.

tumors (50%), and eight in stage 4a/4s tumors (57%). In contrast, the loss of PTEN transcript expression was observed only in four of 44 specimens (Figure 6), supporting previous evidences of low frequent *PTEN* deletion (0–5%) in human neuroblastomas (Moritake *et al.*, 2001; Munoz *et al.*, 2004). These observations, which indicate frequent inactivation of *PICT-1* gene expression in neuroblastoma and the role of PICT-1 in regulating cellular functions, suggest that PICT-1 is a potential causal factor in particular type of human tumor, such as neuroblastoma.

DISCUSSION

In this study, we have demonstrated that PICT-1 down-regulation in HeLa cells induces the activation of PIP_3 downstream kinases and promotes cell proliferation and survival (Figures 1–3). These results, together with our previous observations, suggest that PTEN down-regulation seems to be the primary effect of the PICT-1 knockdown and major cause of these phenomena. We previously observed that the PICT-1 knockdown in MCF7 cells reduced the phosphorylation of PTEN at serine-380, one of the phosphorylation sites in the carboxyl-terminal region of PTEN, and that the reduction in the serine-380 phosphorylation was critical for the PTEN protein stability. Several studies have shown that the carboxyl-terminal phosphorylation of PTEN, including the serine-380 phosphorylation, has diverse effects in addition to promoting PTEN protein stability (Vazquez *et al.*, 2000; Vazquez *et al.*, 2001; Miller *et al.*, 2002; Das *et al.*, 2003; Valiente *et al.*, 2005); therefore, the underlying biochemistry of how the PICT-1 knockdown exerts its effect onto cell functions could be very complex. For example, the carboxyl-terminal phosphorylation is absolutely required to maintain the cellular level of PTEN; however, the phosphorylation also inhibits PTEN phosphatase activity and targeting to the plasma membrane, both of which are essential for its biological function. Reduced phosphorylation resulted from the PICT-1 inactivation could augment the PTEN function by facilitating its membrane localization and the phosphatase activity. However, it is also pronounced that the PICT-1 inactivation eventually unstabilizes PTEN protein and induces its rapid degradation. Extensive decrease in PTEN protein levels may overcome the stimulatory effects caused by reduced phosphorylation, thereby resulting in a loss of PTEN function. It is of note that the effect of the PICT-1 knockdown on the serine-380 phosphorylation in HeLa cells was less obvious, compared with that observed in MCF7 cells (our unpublished data). Although the reason for

this discrepancy is unknown, this might contribute to shift the balance in favor of the inhibition toward the PTEN function by the PICT-1 knockdown. Our result indeed indicates that relatively small change (30–40% reduction; Figure 1) in the expression level of PTEN protein seemed to be enough to down-regulate PTEN function and give severe impact on the PIP_3 signals in HeLa cells. This observation further indicates that PTEN functions in a dose-dependent manner in HeLa cells, which seem to be very sensitive to the alteration in PTEN protein levels. In support of this notion, haploinsufficiency of *PTEN* has been recently suggested to affect several signaling pathways and tumor progression in mouse models (Di Cristofano *et al.*, 1998, 1999; Sun *et al.*, 1999; Kwabi-Addo *et al.*, 2001; Fox *et al.*, 2002; Xiao *et al.*, 2002; Moody *et al.*, 2004; Ma *et al.*, 2005; Manning *et al.*, 2005), indicating a dose-dependent effect of PTEN on diverse cellular functions in vivo. These data collectively raise the possibility that the regulatory system for PTEN protein levels, such as the PICT-1–PTEN system, may function as more dynamic regulatory system and participate in PTEN-mediated diverse signaling pathways in addition to maintaining PTEN protein in cells.

We have also demonstrated that PICT-1 down-regulation promotes the tumorigenic transformation of cells (Figure 4) and that impaired PICT-1 expression is associated with PTEN down-regulation in human neuroblastoma (Figure 5). Intriguingly, *PTEN* gene disruption is uncommon and not the major underlying cause of human neuroblastoma (Moritake *et al.*, 2001; Munoz *et al.*, 2004), whereas previous report (Mora *et al.*, 2001) and our observations (Figures 5 and 6) indicate frequent inactivation of *PICT-1* gene expression in this tumor. This mutually exclusive tissue/tumor specificity represented by *PICT-1* and *PTEN* lesions may expand and emphasize the importance of PTEN in tumorigenesis. The impairment in the *PICT-1* gene may result in PTEN inactivation without any alteration in *PTEN* gene and potentially gives the same impact on cellular functions as impaired *PTEN*. Significant population of neuroblastoma indeed displays these characteristics (Figures 5 and 6), with which tumorigenesis might proceed in a PTEN-dependent manner despite no *PTEN* gene alteration. In addition, low or absent PTEN protein expression, even in the presence of PTEN mRNA, has been observed in several leukemia cell lines (Dahia *et al.*, 1999). Furthermore, human nonsmall-cell lung cancer displays inconsistent correlation of PTEN protein down-regulation and genetic/epigenetic alteration in the *PTEN* gene (Marsit *et al.*, 2005). It could be conceivable that impaired regulatory system for PTEN protein stability may participate in the genesis and/or the progression of these human tumors. These results together suggest a novel itinerary for the tumorigenic transformation that is PTEN dependent but no longer requires *PTEN* gene alterations. Expanded genetic analyses of PICT-1 to identify its implication in human tumors are currently under investigation. Further study will be required to understand the mechanism of how tumorigenesis proceeds by the PICT-1 inactivation and how PICT-1 controls cell fate in PTEN-dependent manner.

ACKNOWLEDGMENTS

This work was supported by Scientific Research Fund of the Ministry of Education, Science, Sports and Culture of Japan. We thank Dr. Jack E. Dixon for providing PC3-Ec-PTEN cells. NIH3T3 cells were provided by Cell Resource Center for Biomedical Research Institute of Development, Aging and Cancer, Tohoku University, Sendai, Japan.

REFERENCES

Ali, I. U., Schriml, L. M., and Dean, M. (1999). Mutational spectra of PTEN/MMAC1 gene: a tumor suppressor with lipid phosphatase activity. J. Natl. Cancer Inst. *91*, 1922–1932.

Cantley, L. C. (2002). The phosphoinositide 3-kinase pathway. Science *296*, 1655–1657.

Cantley, L. C., and Neel, B. G. (1999). New insights into tumor suppression: PTEN suppresses tumor formation by restraining the phosphoinositide 3-kinase/AKT pathway. Proc. Natl. Acad. Sci. USA *96*, 4240–4245.

Dahia, P. L., *et al.* (1999). PTEN is inversely correlated with the cell survival factor Akt/PKB and is inactivated via multiple mechanisms in haematological malignancies. Hum. Mol. Genet. *8*, 185–193.

Das, S., Dixon, J. E., and Cho, W. (2003). Membrane-binding and activation mechanism of PTEN. Proc. Natl. Acad. Sci. USA *100*, 7491–7496.

Di Cristofano, A., Kotsi, P., Peng, Y. F., Cordon-Cardo, C., Elkon, K. B., and Pandolfi, P. P. (1999). Impaired Fas response and autoimmunity in $Pten^{+/-}$ mice. Science *285*, 2122–2125.

Di Cristofano, A., and Pandolfi, P. P. (2000). The multiple roles of PTEN in tumor suppression. Cell *100*, 387–390.

Di Cristofano, A., Pesce, B., Cordon-Cardo, C., and Pandolfi, P. P. (1998). Pten is essential for embryonic development and tumour suppression. Nat. Genet. *19*, 348–355.

Fox, J. A., Ung, K., Tanlimco, S. G., and Jirik, F. R. (2002). Disruption of a single Pten allele augments the chemotactic response of B lymphocytes to stromal cell-derived factor-1. J. Immunol. *169*, 49–54.

Hartmann, C., Johnk, L., Kitange, G., Wu, Y., Ashworth, L. K., Jenkins, R. B., and Louis, D. N. (2002). Transcript map of the 3.7-Mb D19S112–D19S246 candidate tumor suppressor region on the long arm of chromosome 19. Cancer Res. *62*, 4100–4108.

Kwabi-Addo, B., Giri, D., Schmidt, K., Podsypanina, K., Parsons, R., Greenberg, N., and Ittmann, M. (2001). Haploinsufficiency of the Pten tumor suppressor gene promotes prostate cancer progression. Proc. Natl. Acad. Sci. USA *98*, 11563–11568.

Lemmon, M. A., and Ferguson, K. M. (2000). Signal-dependent membrane targeting by pleckstrin homology (PH) domains. Biochem. J. *350*, 1–18.

Leslie, N. R., and Downes, C. P. (2004). PTEN function: how normal cells control it and tumour cells lose it. Biochem. J. *382*, 1–11.

Li, Z., *et al.* (2005). Regulation of PTEN by Rho small GTPases. Nat. Cell Biol. *7*, 399–404.

Lu, Y., *et al.* (2003). Src family protein-tyrosine kinases alter the function of PTEN to regulate phosphatidylinositol 3-kinase/AKT cascades. J. Biol. Chem. *278*, 40057–40066.

Ma, L., Teruya-Feldstein, J., Behrendt, N., Chen, Z., Noda, T., Hino, O., Cordon-Cardo, C., and Pandolfi, P. P. (2005). Genetic analysis of Pten and Tsc2 functional interactions in the mouse reveals asymmetrical haploinsufficiency in tumor suppression. Genes Dev. *19*, 1779–1786.

Maehama, T., and Dixon, J. E. (1998). The tumor suppressor, PTEN/MMAC1, dephosphorylates the lipid second messenger, phosphatidylinositol 3,4,5-trisphosphate. J. Biol. Chem. *273*, 13375–13378.

Manning, B. D., Logsdon, M. N., Lipovsky, A. I., Abbott, D., Kwiatkowski, D. J., and Cantley, L. C. (2005). Feedback inhibition of Akt signaling limits the growth of tumors lacking Tsc2. Genes Dev. *19*, 1773–1778.

Marsit, C. J., Zheng, S., Aldape, K., Hinds, P. W., Nelson, H. H., Wiencke, J. K., and Kelsey, K. T. (2005). PTEN expression in non-small-cell lung cancer: evaluating its relation to tumor characteristics, allelic loss, and epigenetic alteration. Hum. Pathol. *36*, 768–776.

Miller, S. J., Lou, D. Y., Seldin, D. C., Lane, W. S., and Neel, B. G. (2002). Direct identification of PTEN phosphorylation sites. FEBS Lett. *528*, 145–153.

Moody, J. L., Xu, L., Helgason, C. D., and Jirik, F. R. (2004). Anemia, thrombocytopenia, leukocytosis, extramedullary hematopoiesis, and impaired progenitor function in $Pten^{+/-}$ $SHIP^{-/-}$ mice: a novel model of myelodysplasia. Blood *15*, 4503–4510.

Mora, J., Cheung, N. K., Chen, L., Qin, J., and Gerald, W. (2001). Loss of heterozygosity at 19q13.3 is associated with locally aggressive neuroblastoma. Clin. Cancer Res. *7*, 1358–1361.

Moritake, H., Horii, Y., Kuroda, H., and Sugimoto, T. (2001). Analysis of PTEN/MMAC1 alteration in neuroblastoma. Cancer Genet. Cytogenet. *125*, 151–155.

Munoz, J., Lazcoz, P., Inda, M. M., Nistal, M., Pestana, A., Encio, I. J., and Castresana, J. S. (2004). Homozygous deletion and expression of PTEN and

DMBT1 in human primary neuroblastoma and cell lines. Int. J. Cancer *109*, 673–679.

Myers, M. P., Pass, I., Batty, I. H., Van der Kaay, J., Stolarov, J. P., Hemmings, B. A., Wigler, M. H., Downes, C. P., and Tonks, N. K. (1998). The lipid phosphatase activity of PTEN is critical for its tumor suppressor function. Proc. Natl. Acad. Sci. USA *95*, 13513–13518.

Okahara, F., Ikawa, H., Kanaho, Y., and Maehama, T. (2004). Regulation of PTEN phosphorylation and stability by a tumor suppressor candidate protein. J. Biol. Chem. *279*, 45300–45303.

Okahara, F., Itoh, K., Ebihara, M., Kobayashi, M., Maruyama, H., Kanaho, Y., and Maehama, T. (2005). Production of research-grade antibody by in vivo electroporation of DNA-encoding target protein. Anal. Biochem. *336*, 138–140.

Smith, J. S., *et al.* (2000a). Alterations of chromosome arms 1p and 19q as predictors of survival in oligodendrogliomas, astrocytomas, and mixed oligoastrocytomas. J. Clin. Oncol. *18*, 636–645.

Smith, J. S., *et al.* (2000b). A transcript map of the chromosome 19q-arm glioma tumor suppressor region. Genomics *64*, 44–50.

Sumitomo, M., Iwase, A., Zheng, R., Navarro, D., Kaminetzky, D., Shen, R., Georgescu, M. M., and Nanus, D. M. (2004). Synergy in tumor suppression by direct interaction of neutral endopeptidase with PTEN. Cancer Cell *5*, 67–78.

Sun, H., Lesche, R., Li, D. M., Liliental, J., Zhang, H., Gao, J., Gavrilova, N., Mueller, B., Liu, X., and Wu, H. (1999). PTEN modulates cell cycle progression and cell survival by regulating phosphatidylinositol 3,4,5,-trisphosphate and Akt/protein kinase B signaling pathway. Proc. Natl. Acad. Sci. USA *96*, 6199–6204.

Valiente, M., Andres-Pons, A., Gomar, B., Torres, J., Gil, A., Tapparel, C., Antonarakis, S. E., and Pulido, R. (2005). Binding of PTEN to specific PDZ domains contributes to PTEN protein stability and phosphorylation by microtubule-associated serine/threonine kinases. J. Biol. Chem. *280*, 28936–28943.

Vanhaesebroeck, B., Leevers, S. J., Ahmadi, K., Timms, J., Katso, R., Driscoll, P. C., Woscholski, R., Parker, P. J., and Waterfield, M. D. (2001). Synthesis and function of 3-phosphorylated inositol lipids. Annu. Rev. Biochem. *70*, 535–602.

Vazquez, F., Grossman, S. R., Takahashi, Y., Rokas, M. V., Nakamura, N., and Sellers, W. R. (2001). Phosphorylation of the PTEN tail acts as an inhibitory switch by preventing its recruitment into a protein complex. J. Biol. Chem. *276*, 48627–48630.

Vazquez, F., Ramaswamy, S., Nakamura, N., and Sellers, W. R. (2000). Phosphorylation of the PTEN tail regulates protein stability and function. Mol. Cell. Biol. *20*, 5010–5018.

Wu, X., Hepner, K., Castelino-Prabhu, S., Do, D., Kaye, M. B., Yuan, X. J., Wood, J., Ross, C., Sawyers, C. L., and Whang, Y. E. (2000a). Evidence for regulation of the PTEN tumor suppressor by a membrane-localized multi-PDZ domain containing scaffold protein MAGI-2. Proc. Natl. Acad. Sci. USA *97*, 4233–4238.

Wu, Y., Dowbenko, D., Spencer, S., Laura, R., Lee, J., Gu, Q., and Lasky, L. A. (2000b). Interaction of the tumor suppressor PTEN/MMAC with a PDZ domain of MAGI3, a novel membrane-associated guanylate kinase. J. Biol. Chem. *275*, 21477–21485.

Xiao, A., Wu, H., Pandolfi, P. P., Louis, D. N., and Van Dyke, T. (2002). Astrocyte inactivation of the pRb pathway predisposes mice to malignant astrocytoma development that is accelerated by PTEN mutation. Cancer Cell *1*, 157–168.

Yu, J. Y., DeRuiter, S. L., and Turner, D. L. (2002). RNA interference by expression of short-interfering RNAs and hairpin RNAs in mammalian cells. Proc. Natl. Acad. Sci. USA *99*, 6047–6052.

Reciprocal expression of CCAAT/enhancer binding proteins α and ß in hepatoblastomas and its prognostic significance

MINORU TOMIZAWA[1,2], HIROSHI HORIE[3], HIDEKI YAMAMOTO[2], TADASHI MATSUNAGA[3], FUMIAKI SASAKI[3], KOHEI HASHIZUME[3], EISO HIYAMA[3], MICHIO KANEKO[3], SACHIYO SUITA[3], HISAMI ANDO[3], YUTAKA HAYASHI[3], NAOMI OHNUMA[3] and AKIRA NAKAGAWARA[2,3]

[1]Department of Medicine and Clinical Oncology, Chiba University Graduate School of Medicine, 1-8-1 Inohana, Chuo-ku, Chiba City, Chiba 260-8670; [2]Division of Biochemistry, Chiba Cancer Center Research Institute, 666-2 Nitona, Chuo-ku, Chiba City, Chiba 260-8717; [3]The Japanese Study Group for Pediatric Liver Tumor, 1-8-1 Inohana, Chuo-ku, Chiba City, Chiba 260-8670, Japan

Received September 27, 2006; Accepted October 30, 2006

Abstract. Hepatoblastoma is one of the common pediatric solid tumors with frequent mutation of the ß-catenin gene which might be an early event of its carcinogenesis. However, the detailed molecular mechanism is still unknown. We studied the expression levels of CCAAT/enhancer binding protein α (C/EBPα) and C/EBPß, which regulate differentiation and growth of embryonic hepatocytes, to establish whether or not they were involved in affecting the clinical behavior of hepatoblastoma. The quantitative real-time reverse transcriptase-PCR revealed that expression of C/EBPα mRNA was significantly up-regulated in tumors 223% (p=0.013) as compared with that in adjacent normal livers, while expression of C/EBPß was down-regulated to 27% (p=0.002). Of interest, the immunohistochemical analysis showed that expression of C/EBPα was higher and that of C/EBPß lower in the poorly differentiated tumor cells than in the well-differentiated cells within the same tumor. Furthermore, high expression of C/EBPα (p=0.047) as well as low expression of C/EBPß (p=0.025) was significantly associated with poor prognosis of the patients. Cox hazard model suggested that expression of C/EBPα and that of C/EBPß were independent indicators to predict the prognosis from age but not from histology. Thus, expression of C/EBP proteins may play an important role in the genesis and clinical behavior of hepatoblastoma probably by inducing different stages of arrest of differentiation.

Correspondence to: Dr Akira Nakagawara, Division of Biochemistry, Chiba Cancer Center Research Institute, 666-2 Nitona, Chuoh-ku, Chiba 260-8717, Japan
E-mail: akiranak@chiba-cc.jp

Key words: hepatoblast, differentiation, Cox proportional hazard ratio

Introduction

Hepatoblastoma (HBL) is an embryonal tumor and derives from the progenitor cells of the infantile or even the fetal liver which may include hepatoblasts or immature hepatocytes (1). Microscopically, HBL is usually composed of a mixture of well-differentiated tumor cells (fetal type) resembling immature hepatocytes and poorly differentiated cells (embryonal type) similar to embryonic cell components with different proportion (1). Moreover, HBL cells are positive for CK-18 and CK-19, bile duct epithelial markers, as well as α-feto-protein (AFP), a hepatocyte marker, suggesting that HBL also has the components with a potential to differentiate into both directions (2,3).

Hepatocyte differentiation is controlled by coordinated transcription factors. Both CCAAT/enhancer binding protein (C/EBP)α and C/EBPß are liver-enriched transcription factors, regulating the expression of liver-specific genes. Expression of C/EBPα is observed on day 9.5 of gestation, and C/EBPß on day17.5 in the fetal liver of rodents, suggesting that they may be involved in hepatocyte differentiation (4). The hepatocytes in C/EBPα-deficient mice resemble the embryonal type of HBL cells which may have bipotential ability to differentiate into hepatocytes and bile duct epithelial cells (5). This indicates that C/EBPα may play a role in the growth regulation of HBL cells. C/EBPα is down-regulated while C/EBPß is up-regulated in the remnant liver after partial hepatectomy (6).

We studied expression of C/EBPα and C/EBPß in primary HBLs and found that they were expressed in an opposite manner in HBL and significantly associated with the patient prognosis.

Materials and methods

Tissue samples and RNA isolation. The patients underwent surgical treatment at various hospitals or institutions under the framework of the Japanese Study Group for Pediatric Liver Tumor (JPLT) between 1991 and 2005. The extent of the disease (stage) was classified according to that of SIOPEL

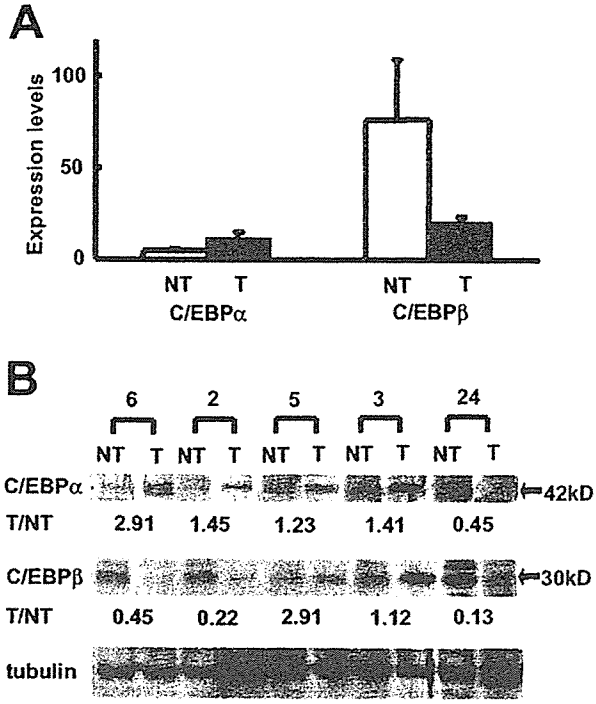

Figure 1. Real-time quantitiative PCR and Western blot analysis of hepatoblastoma with C/EBPα and C/EBPß. (A) Expression levels of C/EBPα and C/EBPß were analyzed with real-time quantitative PCR (x1000) (mean ± standard error). NT, non-tumorous tissue; T, tumorous tissue; n=24. (B) Western blot analysis was performed with representative patients (patient numbers; 6, 2, 5, 3 and 24). The intensities of C/EBPα (42 kD) and C/EBPß (30 kD) proteins expression were normalized against α-tubulin, and the ratio of T to NT was calculated. T/NT, a ratio of the C/EBP expression level in tumorous tissue divided by that in non-tumorous tissue.

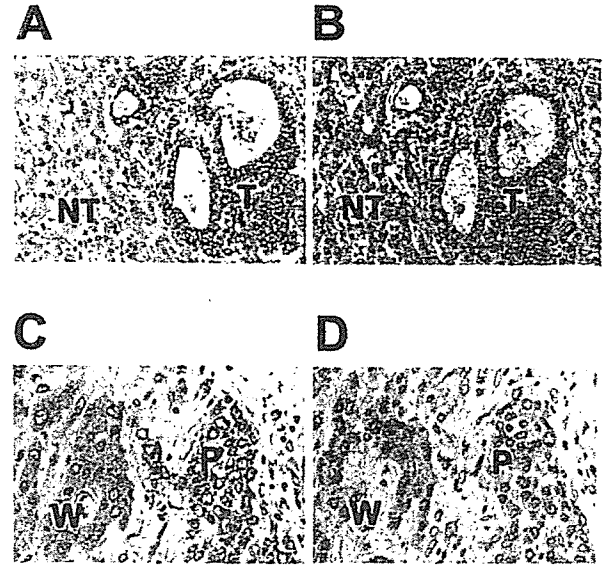

Figure 2. Immunohistochemistry of C/EBPα and C/EBPß in hepatoblastomas. Surgical specimens were immunohistochemically stained with anti-C/EBPα or -C/EBPß antibody. (A) C/EBPα was weakly positive in the cytoplasm and nuclei of normal hepatocytes in non-tumorous tissues (NT). C/EBPα was strongly positive in the cytoplasm and the nuclei of tumor cells (T). (B) C/EBPß was strongly positive in the cytoplasm and nuclei of hepatocytes (NT). C/EBPß was weakly positive in the cytoplasm of tumor cells. (T) (C) C/EBPα was more strongly positive in the cytoplasm of poorly differentiated tumor cells (P) than in that of well differentiated tumor cells (W). (D) C/EBPß was more weakly positive in the cytoplasm of poorly differentiated tumor cells (P) than in that of well differentiated tumor cells (W). Original magnification: x100 (A and B), x400 (C and D).

(7). Histopathology of HBL was according to the classification by the Japanese Society of Pathology which includes well differentiated (fetal) and poorly differentiated (embryonal) types. With informed consent, tumor tissues and their corresponding normal liver tissues were obtained at surgery, immediately frozen, and stored at -80°C until use. Frozen tumor tissues were obtained from 46 patients with HBL, and corresponding normal liver tissues were available from the rejected tissues of 24 patients. All specimens used in this study were provided by the Tissue Bank of JPLT. The JPLT Review Board as well as the Chiba Cancer Center institutional committee approved the analysis with the specimens. Total RNA was prepared by the conventional guanidine thiocyanate-phenol-chloroform procedure.

Real-time quantitative PCR. First-strand cDNA was prepared with 5 μg of total RNA from the surgical specimens, with 200 units of Superscript II reverse transcriptase (Invitrogen Corp., Carlsbad, CA), and 160 pmol of random primers (Takara, Ohtsu, Japan). Synthesized cDNA was subjected to a quantitative real-time PCR (PE Biosystems, Foster City, CA) (8). The primers for C/EBPα were 5'-CGGACTTGG TGCGTCTAAG-3' for 5', 5'-GAGGCAGGAAACCTCC AAAT-3' for 3', and 5'-GAGGCAGGAAACCTCCAAAT-3' for the detection probe; the primers for C/EBPß were 5'-AG CGCGGCGACGAGTACAAGATC-3' for 5', 5'-ACCTTGT GCTGCGTCTCCA-3' for 3', and 5'-CGCGAGCGCAACA ACATCGC-3' for the detection probe. Taq-Man ß-actin control reagents (Perkin Elmer Inc., Wellesley, MA) were used for the amplification of ß-actin as recommended by the manufacturer.

Immunohistochemistry and Western blot analysis. Nine HBL tissues were used for immunohistochemistry, and 5 paired (HBL tissue and its adjacent normal tissue) samples were used for Western blot analysis. Primary antibodies were polyclonal rabbit anti-rat C/EBPα (1:100 dilution, Santa Cruz Biotechnology Inc., Santa Cruz, CA), polyclonal rabbit anti-rat C/EBPß (1:100, dilution, Santa Cruz Biotechnology Inc.), and mouse monoclonal anti-α-tubulin antibody (Lab Vision, Fremont, CA). The exposed films from Western blot analysis were scanned, and the images were analyzed with the software program ImageJ 1.34s (NIH, Bethesda, MD).

Statistical analysis. Kaplan-Meier survival curves were calculated, and survival distributions were compared using the log-rank test. Proportional Cox regression models were used to explore associations among C/EBPα, C/EBPß, age, stage, alpha-feto protein, pathology, and survival. Statistical significance was declared at P-value <0.05. Statistical analysis was performed using Stata 7.0 (Stata Corp., College Station, TX).

Results

The expression levels of C/EBPα and C/EBPß mRNA were measured in primary HBLs and their adjacent normal liver tissues by using quantitative real-time RT-PCR (Fig. 1A).

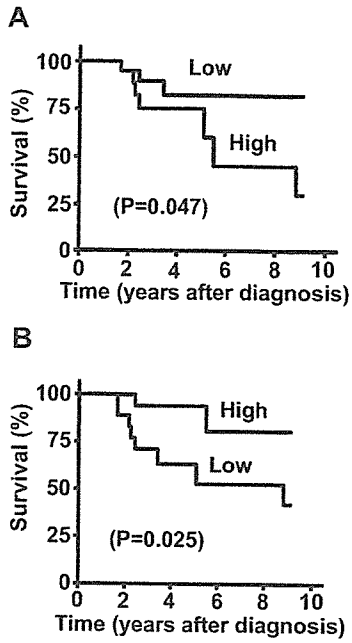

Figure 3. Kaplan-Meier survival curves for patients with hepatoblastoma. Survival of patients with hepatoblastoma after surgery was analyzed (Kaplan-Meier). Patients were divided into two groups for each factor. Patients with higher expression levels of C/EBPα than the median (A) (P=0.047), and lower expression levels of C/EBPß than the median (B) (P=0.025) were associated with shorter survival. P-value for log-rank test is shown in parentheses; n=46.

Table I. Proportional Cox regression models using C/EBPα and C/EBPß and dichotomous factors of age and pathology.

Model	Factor	HR (95% C.I.)	P-value
A	C/EBPα	3.57 (0.91-14.0)	0.068
B	C/EBPß	0.20 (0.04-0.96)	0.044
C	Age	0.27 (0.07-1.02)	0.054
D	Pathology	13.5 (1.70-107)	0.014
E	C/EBPα	4.14 (1.04-16.5)	0.044
	C/EBPß	0.18 (0.04-0.86)	0.031
F	C/EBPα	5.66 (1.32-24.2)	0.019
	C/EBPß	0.17 (0.04-0.81)	0.027
	Age	0.15 (0.03-0.76)	0.022
G	C/EBPα	2.30 (0.56-9.41)	0.25
	C/EBPß	0.40 (0.08-2.07)	0.28
	Pathology	7.95 (0.87-72.6)	0.066

HR, hazard ratio showing the relative risk of death of the first category relative to the second; parenthesis, 95% confidence interval (C.I.); C/EBPα and C/EBPß, high vs. low expression levels of C/EBPα and C/EBPß in tumor with real-time quantitative PCR; n=46.

The C/EBPα expression was significantly high in the tumors (mean ± SEM: 11.6±3.2, n=24) as compared with that in the normal livers (5.1±0.9, n=24; p=0.013). On the other hand, the expression of C/EBPß was significantly lower in HBL tissues (20.4±2.7, n=24) than that in the normal liver tissues (75.8±33, n=24; p=0.002). To confirm these results, we next measured expression levels of C/EBPα and C/EBPß proteins in 5 paired samples of tumor and its corresponding normal liver by Western blot analysis. The data obtained showed a tendency of up-regulation of C/EBPα and down-regulation of C/EBPß in the tumor tissues as compared with the paired normal livers (Fig. 1B).

Fig. 2 shows immunohistochemical stainings of primary HBLs. C/EBPα was weakly positive in the cytoplasm and nuclei of normal hepatocytes, and strongly positive mainly in the cytoplasm of tumor cells (Fig. 2A). By contrast, C/EBPß was rather positive in the cytoplasm and nuclei of hepatocytes in the adjacent normal livers, whereas it was weakly positive in the cytoplasm of the tumor cells (Fig. 2B). In the same tumor tissues, C/EBPα was more strongly positive in the poorly differentiated tumor cells than the adjacent well-differentiated tumor cells (Fig. 2C). C/EBPß was weakly positive in the poorly differentiated tumor cells, whereas it was almost negative in the well-differentiated tumor cells (Fig. 2D).

The Kaplan-Meier cumulative survival curves are shown in Fig. 3. The high levels of expression of C/EBPα mRNA were significantly associated with poor patient survival (68.2% 5-year survival rate, n=22, vs. 87.5%, n=24; p=0.047), whereas high levels of expression of C/EBPß mRNA were significantly correlated with favorable prognosis (92.6% 5-year survival rate, n=27, vs. 57.9%, n=19; p=0.025). Univariate Cox regression analysis of 46 patients with HBL showed that expression of C/EBPß (high vs. low expression; p=0.044), age (<1-year vs. ≥1-year; p=0.054) and histopathology (well vs. poorly differentiated; p=0.014) were significant indicators of the prognosis, while expression of C/EBPα (p=0.068) was marginally significant as a prognostic factor of HBLs (Table I). Multivariate analysis using Cox model showed that C/EBPα and C/EBPß were significantly related to survival in a model jointly with each factor (P<0.05, model E). C/EBPα and C/EBPß were significantly related to survival (P<0.047) even after controlling age (P=0.022, model F). Finally, since 9 out of 10 deceased patients had poorly differentiated histopathology, C/EBPα and C/EBPß would lose significance in a model including pathology (model G).

Discussion

The basic studies of hepatoblastoma have recently provided important information to understanding of genesis and progression of HBL. The ß-catenin gene was discovered to be mutated and translocated into the cellular nucleus (9). However, high frequency of aberration of the Wnt signaling appeared to be an early event and the ß-*catenin* mutation itself did not have prognostic significance (8). The studies using comparative genomic hybridization (CGH) presented an interesting pattern of the chromosomal aberrations in HBLs (10). The comprehensive cDNA project of HBLs has also given some insights into the understanding of the molecular aspect of HBLs by identifying a large number of

differentially expressed genes between the HBL tumors and their corresponding normal livers, that indentified Plk1 as a highly expressed gene in HBLs (11). However, expression of most of the genes was not predictive for prognosis.

The C/EBPα gene is mapped to chromosome 19q, which is often gained in HBLs and has been found to be up-regulated in HBLs (12). However, the gene is mutated in acute myeloid leukemia and is often down-regulated in some other cancers, suggesting that C/EBPα may function as a tumor suppressor (13,14). In addition, our previous study suggested that both C/EBPα and C/EBPß were down-regulated in hepatocellular carcinomas as compared with the adjacent non-tumorous liver tissues (15). These suggest that C/EBPα may play a different role in HBLs from other cancers.

C/EBPß was down-regulated in HBLs as compared with the corresponding normal livers and correlated with poor prognosis in the HBL patients, that was similar to HCC and other cancers (15,16). Buck *et al* reported that overexpression of C/EBPß in HepG2 cells, a human HCC cell line, suppressed proliferation of the cells (17). Therefore, C/EBPß might function as a tumor suppressor in HBL cells. In addition, C/EBPß may also play a role in regulating differentiation of HBL cells because the gene is expressed in mature hepatocytes and is reported to be indispensable for induction of the lever-specific genes.

Thus, both C/EBPα and C/EBPß may play important roles in regulating growth and differentiation of HBLs. Moreover, a small amount of tumor biopsy samples could be used for measuring the mRNA expression levels of both genes for predicting aggressiveness of the HBL tumors.

Acknowledgements

This study was supported by the Japan Society for the Promotion of Science (JSPS), the Ministry of Education, Science, Sports, and Culture, and the Ministry of Health, Labour, and Welfare. We thank Dr Hajime Takayasu, Dr Shin-ichi Yamada, and Dr Miki Ohira for their advice.

References

1. Ishak KG and Glunz PR: Hepatoblastoma and hepatocarcinoma in infancy and childhood. Report of 47 cases. Cancer 20: 396-422, 1967.
2. Pietsch T, Fonatsch C, Albrecht S, Maschek H, Wolf HK and von Schweinitz D: Characterization of the continuous cell line HepT1 derived from a human hepatoblastoma. Lab Invest 74: 809-818, 1996.
3. Ruck P, Xiao JC and Kaiserling E: Small epithelial cells and the histogenesis of hepatoblastoma. Electron microscopic, immuno-electron microscopic, and immunohistochemical findings. Am J Pathol 148: 321-329, 1996.
4. Shiojiri N, Takeshita K, Yamasaki H and Iwata T: Suppression of C/EBP alpha expression in biliary cell differentiation from hepatoblasts during mouse liver development. J Hepatol 41: 790-798, 2004.
5. Tomizawa M, Garfield S, Factor V and Xanthopoulos KG: Hepatocytes deficient in CCAAT/enhancer binding protein alpha (C/EBP alpha) exhibit both hepatocyte and biliary epithelial cell character. Biochem Biophys Res Commun 249: 1-5, 1998.
6. Flodby P, Antonson P, Barlow C, Blanck A, Porsch-Hallstrom I and Xanthopoulos KG: Differential patterns of expression of three C/EBP isoforms, HNF-1, and HNF-4 after partial hepatectomy in rats. Exp Cell Res 208: 248-256, 1993.
7. Perilongo G, Shafford E and Plaschkes J: SIOPEL trials using preoperative chemotherapy in hepatoblastoma. Lancet Oncol 1: 94-100, 2000.
8. Takayasu H, Horie H, Hiyama E, *et al*: Frequent deletions and mutations of the beta-catenin gene are associated with over-expression of cyclin D1 and fibronectin and poorly differentiated histology in childhood hepatoblastoma. Clin Cancer Res 7: 901-908, 2001.
9. Park WS, Oh RR, Park JY, *et al*: Nuclear localization of beta-catenin is an important prognostic factor in hepatoblastoma. J Pathol 193: 483-490, 2001.
10. Weber RG, Pietsch T, von Schweinitz D and Lichter P: Characterization of genomic alterations in hepatoblastomas. A role for gains on chromosomes 8q and 20 as predictors of poor outcome. Am J Pathol 157: 571-578, 2000.
11. Yamada S, Ohira M, Horie H, *et al*: Expression profiling and differential screening between hepatoblastomas and the corresponding normal livers: identification of high expression of the PLK1 oncogene as a poor-prognostic indicator of hepatoblastomas. Oncogene 23: 5901-5911, 2004.
12. Gray SG, Kytola S, Matsunaga T, Larsson C and Ekstrom TJ: Comparative genomic hybridization reveals population-based genetic alterations in hepatoblastomas. Br J Cancer 83: 1020-1025, 2000.
13. Pabst T, Mueller BU, Zhang P, *et al*: Dominant-negative mutations of CEBPA, encoding CCAAT/enhancer binding protein-alpha (C/EBPalpha), in acute myeloid leukemia. Nat Genet 27: 263-270, 2001.
14. Halmos B, Huettner CS, Kocher O, Ferenczi K, Karp DD and Tenen DG: Down-regulation and antiproliferative role of C/EBPalpha in lung cancer. Cancer Res 62: 528-534, 2002.
15. Tomizawa M, Watanabe K, Saisho H, Nakagawara A and Tagawa M: Down-regulated expression of the CCAAT/enhancer binding protein alpha and beta genes in human hepatocellular carcinoma: a possible prognostic marker. Anticancer Res 23: 351-354, 2003.
16. Oh HS and Smart RC: Expression of CCAAT/enhancer binding proteins (C/EBP) is associated with squamous differentiation in epidermis and isolated primary keratinocytes and is altered in skin neoplasms. J Invest Dermatol 110: 939-945, 1998.
17. Buck M, Turler H and Chojkier M: LAP (NF-IL-6), a tissue-specific transcriptional activator, is an inhibitor of hepatoma cell proliferation. EMBO J 13: 851-860, 1994.

Pathology International 2006; **56**: 543–548 doi:10.1111/j.1440-1827.2006.02003.x

Case Report

Desmoplastic small cell tumor of soft tissue: Molecular variant of *EWS-WT1* chimeric fusion

Minoru Hamazaki,[1] Hajime Okita,[2] Jun-ichi Hata,[3] Shin-ichi Shimizu,[4] Hiroshi Kobayashi,[4] Katsuhiko Aoki[5] and Taemi Nara[6]

Departments of [1]Pathology, [5]Radiology and [6]Oncology, Shizuoka Children's Hospital, Shizuoka, [2]Department of Developmental Biology, National Research Institute for Child Health and Development, [3]National Center for Child Health and Development, Tokyo and [4]Department of Pathology, Seirei Hamamatsu General Hospital, Hamamatsu, Japan

A 7-year-old girl was hospitalized because of a tumorous mass in her left periorbital region. The tumor was removed by local excision. The soft-part tumor recurred in the parotid gland region 4 months later, and a second recurrence was noted on the left side of the neck 3 years and 3 months thereafter. The patient had not received chemotherapy or local irradiation. Histological and immunohistochemical examinations of the recurrent masses revealed morphological characteristics of small cell proliferation with desmoplastic stroma that were similar to those of the initial tumor. The cellular components showed immunoreactivity for desmin, cytokeratin, vimentin, and epithelial membrane antigen in part, but the cells were negative for myogenin, CD99, and neuron-specific enolase. These findings suggested a diagnosis of desmoplastic small cell tumor, despite its extra-abdominal location. The histological diagnosis was confirmed by reverse transcriptase polymerase chain reaction, which demonstrated an *EWS-WT1* chimeric fusion gene. An in-frame fusion of *EWS* exon 9 and *WT1* exon 8 was subsequently identified by cloning and sequencing. The chimeric fusion gene might be related to the tissue-specific phenotype of desmoplastic small cell tumors, although further investigation of this speculation is necessary.

Key words: desmoplastic small cell tumor, *EWS-WT1* fusion transcript, extra-abdominal

Desmoplastic small cell tumor (DSCT) occurs usually in the intra-abdominal region of children or adolescents and consists of proliferating small cells with a desmoplastic stroma. DSCT is also characterized by the presence of an *EWS-WT1* chimeric fusion transcript, typically confirmed by reverse transcriptase–polymerase chain reaction (RT-PCR). Tumors with similar histological appearances have been reported in other soft tissues,[1] but such tumors are extremely rare. Here, we describe a patient with a desmoplastic small cell tumor that developed primarily in the orbital soft tissue.

CLINICAL SUMMARY

A 7-year-old girl complained of an insidious swelling in the soft tissue of her left upper eyelid. On hospitalization, a reconstructed CT image revealed a partially calcified, low-density mass in the upper lateral aspect of the left orbital region (Fig. 1). The mass was excised surgically. The patient was not treated with systemic chemotherapy or local irradiation.

Four months after the initial surgery, a local recurrence was detected in the left periorbital region. A CT image revealed an irregular mass, measuring 26 × 20 mm in greatest diameter, with central low-density and calcified foci; the mass was located near the upper aspect of the left parotid gland (Fig. 1). Systemic gallium citrate scintigraphy demonstrated an abnormally localized accumulation at the mass lesion, but no distant metastases were noted. The local tumor was completely re-excised surgically, and the patient was carefully followed thereafter. Chemotherapy or irradiation was not performed.

Three years and 3 months later, at the age of 11 years, the patient was again hospitalized because of a second recurrence in her left lower neck region. CT showed a tumorous lesion located between the left lower margin of the parotid gland and the piriform fossa. The main cervical recurrent tumor and nodal metastases were removed. The tumorous tissue weighed 38.9 g in total. The patient has been followed for 8 months and has shown no signs of local recurrence,

Correspondence: Minoru Hamazaki, MD, Department of Pathology, Shizuoka Children's Hospital, 860 Urushiyama, Aoi-ku, Shizuoka 420-8660, Japan. Email: mhamasan@sch.pref.shizuoka.jp

Received 13 March 2006. Accepted for publication 1 May 2006.

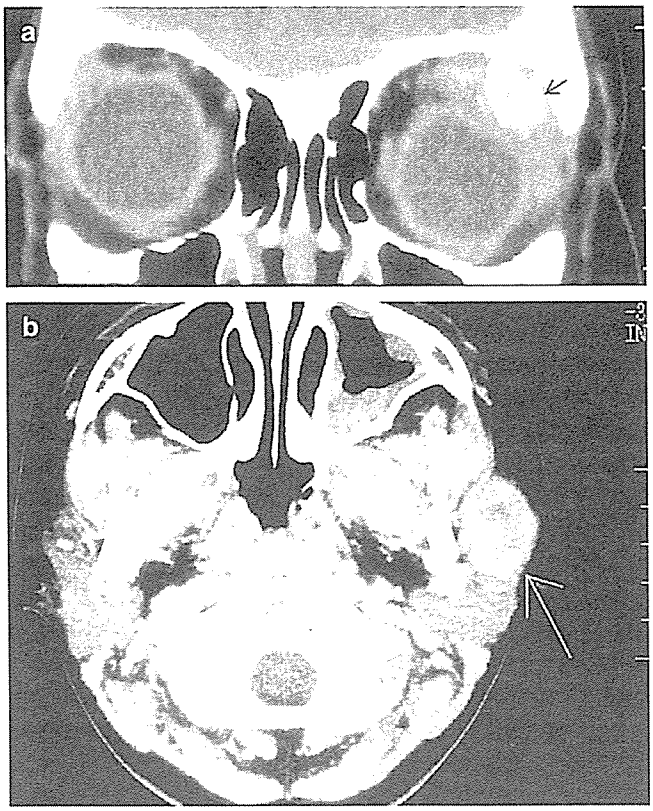

Figure 1 Radiological appearance. (**a**) The initial tumor mass (arrow) is visible in the left upper lateral aspect of the orbital region as a partially calcified, low-density mass on a CT image. (**b**) CT of the first recurrence showing an irregular mass (arrow) with a central low-density area near the upper aspect of the left parotid gland.

although the possibility of future recurrence cannot be ruled out.

PATHOLOGICAL FINDINGS

A conventional morphological examination was performed using formalin-fixed paraffin sections stained with HE. Histological examination of the primary tumor suggested an epithelial neoplasm, like a lacrimal gland carcinoma or an adenoid cystic carcinoma, or a rhabdomyosarcoma or metastasis of an abdominal tumor. The first recurrent tumor was characterized by conspicuously atypical small cell proliferation, forming solid cellular nodules or trabecular, basalioid epithelial lesions, and was accompanied by prominent interstitial fibrous intervention (Fig. 2). The tumorous tissue was intermingled with the ducts of the parotid gland, and the tumor itself was located adjacent to the serous acini of the parotid gland. The second recurrent main tumor exhibited diffuse cellular proliferation but did not have a desmoplastic stroma. The nodal metastases in the lower portion of the left neck, however, exhibited a distinct desmoplastic morphology similar to that of the first recurrent tumor. These histological findings were consistent with a desmoplastic small cell tumor of soft tissue with divergent differentiation, and were almost identical to those of the initial orbital tumor.

Immunohistochemical study

The immunohistochemical investigation was performed using formalin-fixed, paraffin-embedded tissues and the streptoavidin–biotin peroxidase indirect method. Primary antibodies were prepared against the following antigens: desmin (clone DE-R-11, diluted 1:50; DakoCytomation, Glostrup, Denmark), cytokeratin (AE1/AE3, diluted 1:50, proteinase K-treated; DakoCytomation), vimentin (Vim3B4, diluted 1:50, microwave-treated; DakoCytomation), epithelial membrane antigen (EMA; E29, diluted 1:50; DakoCytomation), myogenin (F5D, diluted 1:50, microwave-treated; DakoCytomation), WT1 (C-19, diluted 1:50, proteinase K-treated; Santa Cruz Biotechnology, Santa Cruz, CA, USA), CD99 (F5D, diluted 1:50; DakoCytomation), sarcomeric actin (α-Sr-1, diluted 1:40; DakoCytomation), CD45 (T29/33, diluted 1:50; DakoCytomation), glial fibrillary acidic protein (GFAP; 6F2, diluted 1:50, microwave-treated; DakoCytomation), neuron-specific enolase (NSE; BBS/NC/VI-H14, diluted 1:50; DakoCytomation), S-100 protein (rabbit polyclonal, diluted 1:400; DakoCytomation), Ki-67 antigen (MIB-1, diluted 1:50, microwave-treated; DakoCytomation), and P53 (PAb240, diluted 1:50, microwave-treated; DakoCytomation).

The solid areas of the first and second recurrent tumors were positive for vimentin, but the trabeculae were negative. In contrast, the trabecular or epithelioid components were positive for EMA, but the solid cellular area was negative. Distinct positive immunoreactivity for desmin and cytokeratin was expressed in the cytoplasm of the small tumor cells in both the solid cellular and trabecular architectures (Fig. 3). No evidence of myogenin, WT1, CD99, sarcomeric actin, CD45, GFAP, NSE, or S-100 protein positivity was seen. Ki-67 labeling index was 40–60% in the solid area of tumor and 10–20% at the trabeculae. P53 labeling index was <1–5%.

Electron microscopy

The electron microscopy specimens were prepared using conventional 2% glutaraldehyde and 1% osmium tetraoxide fixation followed by epoxy embedding. Ultrathin sections stained with uranyl acetate and lead citrate were then observed using a JEM 1010 transmission electron microscope (JEOL, Tokyo, Japan).

The tumor cells were characterized by prominent desmosome-type intercellular junctions with tonofilaments (Fig. 4). A small amount of intermediate fibrils without striated muscle

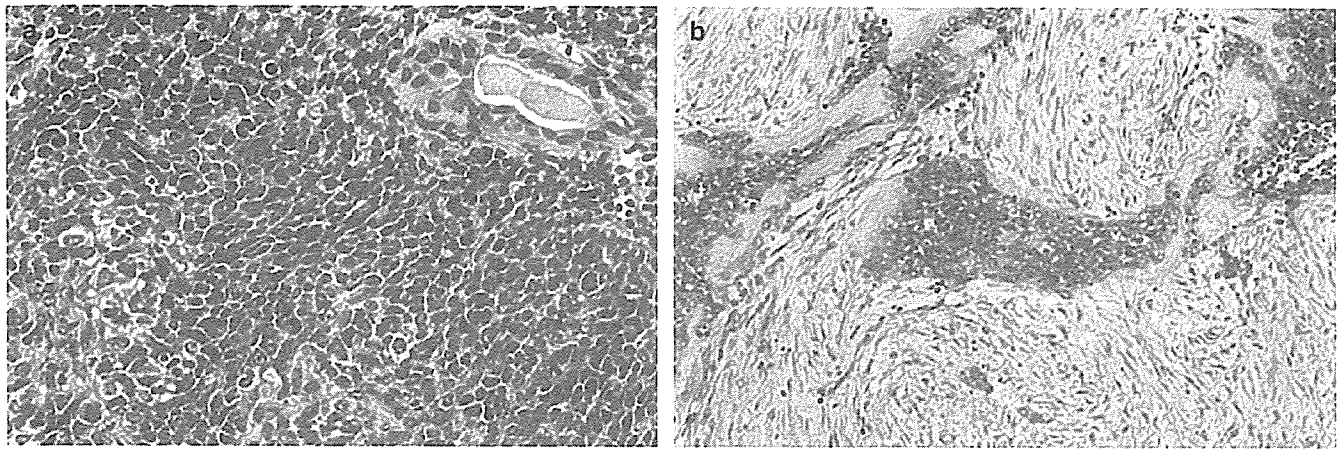

Figure 2 Histological findings. (**a**) Conspicuous proliferation of small atypical cells with increased mitotic figures is apparent. A salivary gland duct is visible at the right of the figure. (**b**) The tumor tissue is characterized by trabecular, epithelioid proliferation surrounded by a hyaline basal structure, with fibrous proliferation in the interstitium.

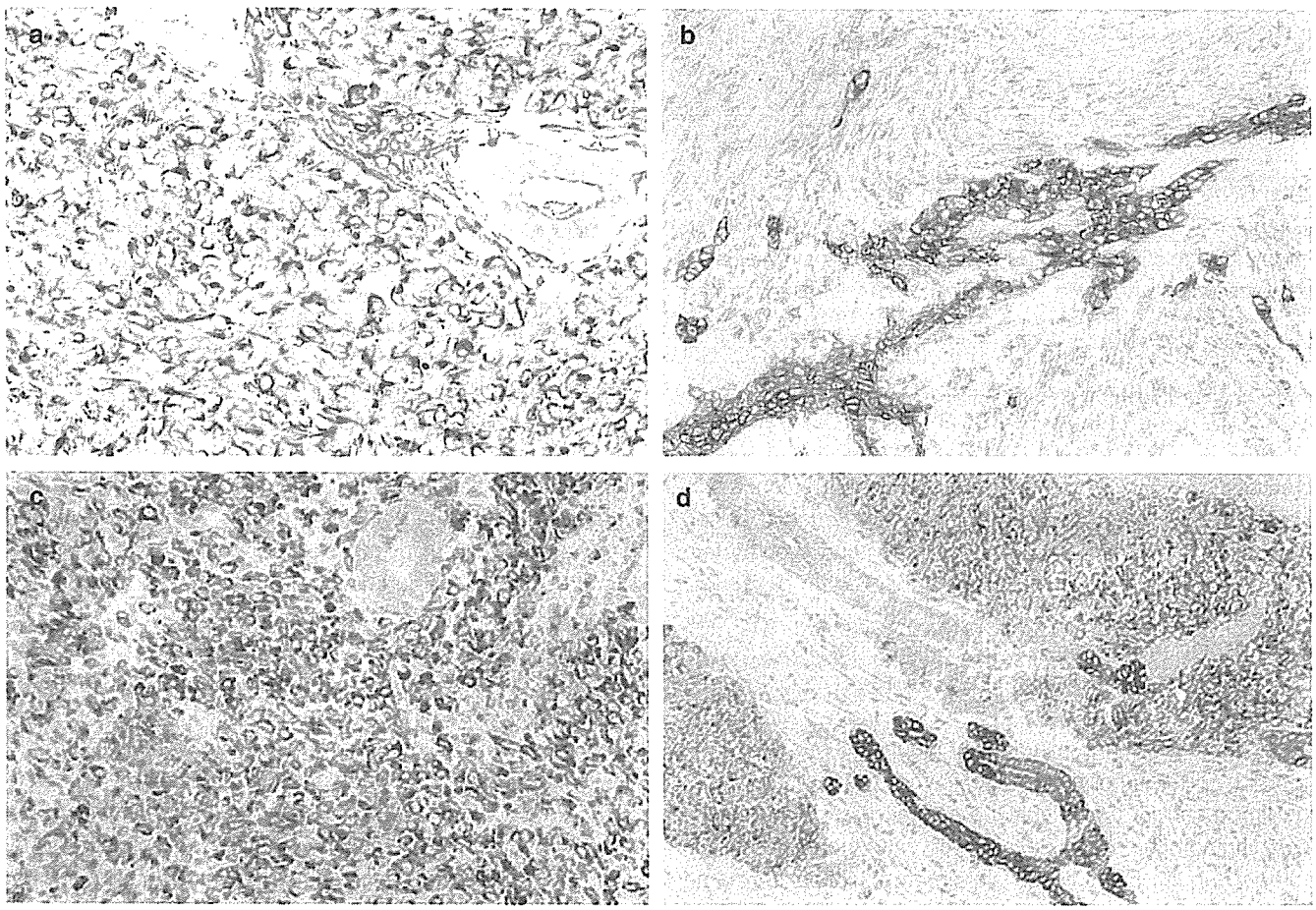

Figure 3 Immunohistochemical findings. (**a**) Vimentin is reactive in the cytoplasm of the tumor cells. (**b**) EMA is positive at the membrane of the tumor cells, especially in the trabecular region. Immunostaining was positive for (**c**) desmin and (**d**) cytokeratin in both solid and trabecular portions of the tumor.